

This document is confidential and is proprietary to the American Chemical Society and its authors. Do not copy or disclose without written permission. If you have received this item in error, notify the sender and delete all copies.

## A Polymer Prodrug Strategy to Switch from Intravenous to Subcutaneous Cancer Therapy for Irritant/Vesicant Drugs

Journal:	<i>Journal of the American Chemical Society</i>
Manuscript ID	Draft
Manuscript Type:	Article
Date Submitted by the Author:	n/a
Complete List of Authors:	<p>Bordat, Alexandre; Institut Galien Paris Sud, Universite Paris Sud, Faculte de Pharmacie            Boissenot, Tanguy; Institut Galien Paris Sud, Universite Paris Sud, Faculte de Pharmacie            Makky, Nada; Université Paris-Saclay, CNRS, Institut Galien Paris-Saclay            Ferrere, Marianne; Université Paris-Saclay, CNRS, Institut Galien Paris-Saclay            Levêque, Manon ; Université Paris-Saclay, CNRS, Institut Galien Paris-Saclay            Denis, Stéphanie; Université Paris-Saclay, CNRS, Institut Galien Paris-Saclay            Garcia-Argote, Sébastien; CEA, iBiTec-S            Carvalho, Olivia; CEA, iBiTec-S            Abadie, Jerome; ONIRIS, AMAROC            Cailleau, Catherine ; Université Paris-Saclay, CNRS, Institut Galien Paris-Saclay            Pieters, Grégory; CEA Direction des Sciences de la Matière, SCBM            Tsapis, Nicolas; Université Paris-Saclay, CNRS, Institut Galien Paris-Saclay            Nicolas, Julien; Université Paris-Saclay, CNRS, Institut Galien Paris-Saclay</p>

SCHOLARONE™  
Manuscripts

1  
2  
3  
4 A Polymer Prodrug Strategy to Switch from  
5  
6  
7  
8  
9 Intravenous to Subcutaneous Cancer Therapy for  
10  
11  
12  
13 Irritant/Vesicant Drugs  
14  
15  
16  
17  
18  
19  
20  
21

22 *Alexandre Bordat,<sup>1,2</sup> Tanguy Boissenot,<sup>1,2</sup> Nada Makky,<sup>1,2</sup> Marianne Ferrere,<sup>1</sup> Manon*  
23  
24 *Levêque,<sup>1</sup> Stéphanie Denis,<sup>1</sup> Sébastien Garcia-Argote,<sup>3</sup> Olivia Carvalho,<sup>3</sup> Jérôme Abadie,<sup>4</sup>*  
25  
26  
27 *Catherine Cailleau,<sup>1</sup> Grégory Pieters,<sup>3</sup> Nicolas Tsapis,<sup>1,\*</sup> Julien Nicolas<sup>1,\*</sup>*  
28  
29  
30  
31  
32  
33  
34  
35  
36  
37

38 <sup>1</sup> Université Paris-Saclay, CNRS, Institut Galien Paris-Saclay, 92296 Châtenay-Malabry, France

39  
40 <sup>2</sup> Present address: Imescia, Université Paris-Saclay, 92296 Châtenay-Malabry, France

41  
42 <sup>3</sup> Université Paris-Saclay, CEA, INRAE, Département Médicaments et Technologies pour la Santé  
43  
44 (DMTS), SCBM, Gif-sur-Yvette, F-91191 France

45  
46 <sup>4</sup> Oniris, Laboniris, Département de Biology, Pathologie et Sciences de l'Aliment, Nantes, France  
47  
48  
49  
50  
51  
52  
53

54 \*To whom correspondence should be addressed.

55  
56 Email: [nicolas.tsapis@universite-paris-saclay.fr](mailto:nicolas.tsapis@universite-paris-saclay.fr) (NT)

57  
58 Email: [julien.nicolas@u-psud.fr](mailto:julien.nicolas@u-psud.fr) (JN)  
59  
60

## Abstract

Chemotherapy is almost exclusively administered via the intravenous (IV) route, which has serious limitations (e.g., patient discomfort, long hospital stays, need for trained staff, high cost, catheter failures, infections). Therefore, the development of effective and less costly chemotherapy that is more comfortable for the patient would revolutionize cancer therapy. While subcutaneous (SC) administration has the potential to meet these criteria, it is extremely restrictive as it cannot be applied to most anticancer drugs, such as irritant or vesicant ones, for local toxicity reasons. Herein, we report a facile, general and scalable approach for the SC administration of anticancer drugs through the design of well-defined hydrophilic polymer prodrugs. This was applied to the anticancer drug paclitaxel (Ptx) as a worst-case scenario due to its high hydrophobicity and vesicant properties (two factors promoting necrosis at the injection site), whereas polyacrylamide (PAAm) was chosen as a hydrophilic polymer for its biocompatibility and stealth properties. A small library of Ptx-based polymer prodrugs was designed by adjusting the nature of the linker (ester, diglycolate and carbonate), and then evaluated in terms of rheological/viscosity properties in aqueous solutions, drug release kinetics in PBS and in murine plasma, cytotoxicity on two different cancer cell lines, acute local and systemic toxicity, pharmacokinetics and biodistribution, and finally their anticancer efficacy. We demonstrated that Ptx-PAAm polymer prodrugs could be safely injected subcutaneously without inducing local toxicity while outperforming Taxol, the commercial formulation of Ptx, thus opening the door to the safe transposition from IV to SC chemotherapy.

## Introduction

Due to population growth and aging, the number of new cancer cases is expected to increase by approximately 70% over the next 20 years.<sup>1-2</sup> As a result, not only will more and more patients have to deal with cancer, but hospital organization will be strained while patients and health care systems will face an increasing financial burden.<sup>3,4</sup> In addition, since chemotherapy is mostly administered intravenously (IV),<sup>5</sup> it is usually accompanied by severe limitations that are directly responsible for patient discomfort and the high cost of cancer treatments: (i) injectable formulations must be prepared in chemotherapy reconstitution units; (ii) administration must be performed by qualified workers at the hospital, often via a central IV route that requires an implantable chamber; (iii) the patient must stay at the hospital during treatment to be monitored for an early detection of infusion-related toxicities and (iv) catheter failures and life-threatening infections often occur.<sup>6-7</sup> Therefore, the development of effective chemotherapy that is more comfortable and less dangerous for the patient and also less costly, to significantly decrease the financial burden on patients and health care systems, represents an urgent and unmet clinical need.

To address this challenge, one can turn to the area of subcutaneous (SC) injectables. SC administration is indeed much more comfortable for the patient than IV administration, as it is less invasive and easy to implement.<sup>8</sup> Also, no hospital stay is required, making home chemotherapy and even self-administration possible.<sup>9</sup> Compared to the oral route, SC administration offers superior bioavailability (>80%), faster and better controlled absorption of the drug, drastically reduced compliance problems and less variability between patients.<sup>10</sup>

The technologies currently developed for the SC administration of small drugs/therapeutic proteins are mainly based on either their direct administration,<sup>10-11</sup> with strategies to increase their aqueous stability (e.g., cyclodextrins, Biochaperone)<sup>12-13</sup> or SC injection volume (e.g., hyaluronidase),<sup>14</sup> or on the injection of drug-loaded nanoscale systems

1  
2  
3 (e.g., hydrogels, nanoparticles, liposomes, lipid prodrugs).<sup>15-17</sup> However, these approaches  
4 cannot be applied to the vast majority of anticancer drugs. The field of SC injectables for cancer  
5 therapy is indeed extremely restricted,<sup>10</sup> because most anticancer drugs (including very  
6 effective ones such as taxanes, vinca alkaloids, doxorubicine, etc.) are irritant or vesicant. They  
7 induce prohibitive local toxicity such as severe irritation and necrosis,<sup>18</sup> which are triggered by  
8 their prolonged retention in SC tissue due to their high lipophilicity. Anticancer drugs are thus  
9 repeatedly internalized by SC cells, causing their death and preventing the healing process.<sup>19-21</sup>

19 Herein, we report the first preclinical development of a general strategy for the SC  
20 administration of irritant/vesicant, anticancer drugs. Our idea is based on the design of water-  
21 soluble polymer prodrugs comprising one anticancer drug molecule attached at the extremity  
22 of a well-defined polyacrylamide (PAAm) chain (Figure 1a). PAAm is an uncharged, highly  
23 water-soluble and biocompatible polymer used in nanomedicine,<sup>22-23</sup> with stealth properties and  
24 also employed as permanent dermal filler (Aquamid®).<sup>24</sup> It thus fully meets the criteria for SC  
25 administration as recommended by Mrsny.<sup>25</sup> To demonstrate the proof of concept, we chose  
26 paclitaxel (Ptx), a representative hydrophobic irritant/vesicant anticancer drug widely used in  
27 the clinic. It was bound to PAAm via a cleavable linker positioned on its C2' hydroxyl group,<sup>26</sup>  
28 resulting in inactive Ptx-based prodrugs (Figure 1b). The prodrugs' characteristics thus: (i)  
29 prevent early release of the drug into the SC tissue; (ii) promote their diffusion throughout the  
30 SC tissue and absorption into blood/lymph capillaries to yield high bioavailability and (iii)  
31 allow the drug to be released into the bloodstream where it can exert its therapeutic activity  
32 (Figure 1c).

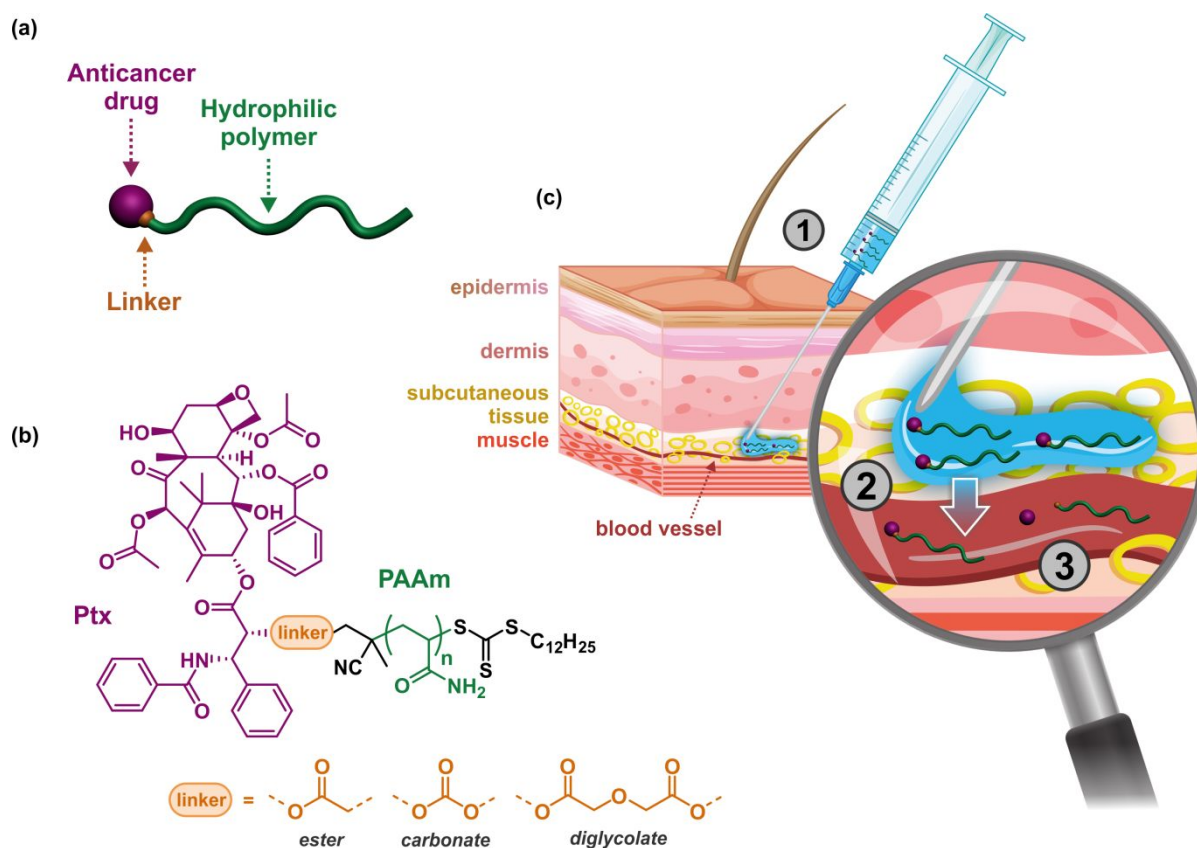


**Figure 1.** (a) Schematic representation of the water-soluble polymer prodrug used in this work. (b) Chemical structure of paclitaxel-linker-polyacrylamide (Ptx-linker-PAAm) polymer prodrugs with three different linkers (i.e., ester, carbonate and diglycolate). (c) Subcutaneous administration of an aqueous solution of Ptx-polymer prodrugs (1), followed by their absorption by the blood/lymph vessels (2) and release of Ptx after linker cleavage (3).

We showed that our strategy is safe as no local toxicity was observed. Precise tuning of the prodrug structure also allowed us to greatly decrease the peak drug concentration ( $C_{\max}$ ), responsible for systemic toxicity,<sup>27</sup> while achieving sustained drug exposure. Importantly, our approach enabled a 3-fold increase of the maximum tolerated dose (MTD) and therefore a greater anticancer efficacy when benchmarked against IV-administered Taxol, the most common commercial formulation of Ptx.

## Materials and methods

### Materials

Acrylamide (AAM) ( $\geq 99\%$ , Sigma-Aldrich) was recrystallized from chloroform. Azobisisobutyronitrile (AIBN) (98%, Sigma-Aldrich) was recrystallized from ethanol. 4-Cyano-4-[(dodecylsulfanylthiocarbonyl)-sulfanyl]pentanoic acid (97%, CDSPA), 4-cyano-4-[(dodecylsulfanylthiocarbonyl)sulfanyl]pentanol (CDP), 4-dimethylaminopyridine ( $\geq 96.5\%$ , DMAP), 1-(3-dimethylaminopropyl)-3-ethylcarbodiimide hydrochloride ( $\geq 98\%$ , EDC.HCl), diglycolic anhydride ( $\geq 96.0\%$ ), RPMI-1640 cell culture medium, insulin from bovine pancreas, Eagle's Minimum Essential Medium (EMEM) and Dulbecco's Modified Eagle Medium/Nutrient Mixture F-12 HAM (DMEM F-12 HAM) were purchased from Sigma-Aldrich and used as received. Paclitaxel (Ptx) was purchased from Carbosynth, [ $^3\text{H}$ ]-Paclitaxel ( $3 \text{ Ci}\cdot\text{mmol}^{-1}$ , 1 mCi) was purchased from Moravek both used as received. Ptx-*diglycolate*-CDP was synthesized as described elsewhere.<sup>28</sup> Deuterated chloroform ( $\text{CDCl}_3$ ) and dimethyl sulfoxide ( $d_6$ -DMSO) were obtained from Eurisotop. Taxol was purchased from Fresenius Kabi France. All solvents were purchased from Sigma-Aldrich at the highest grade.

### Analytical methods

*Nuclear magnetic resonance (NMR) spectroscopy.*  $^1\text{H}$  NMR and  $^{13}\text{C}$  NMR spectroscopy of small molecules was performed in 5 mm diameter tubes in deuterated chloroform ( $\text{CDCl}_3$ ) on a Bruker Avance 300 spectrometer operating at 300 MHz ( $^1\text{H}$ ) or 75 MHz ( $^{13}\text{C}$ ) at room temperature. For  $^1\text{H}$  NMR spectroscopy of polymers, acquisition was performed in 5 mm diameter tubes in  $d_6$ -DMSO at 70 °C (128 scans) on a Bruker Avance 3 HD 400 spectrometer operating at 400 MHz. NMR determination of the number-average molar mass ( $M_{n,\text{NMR}}$ ) of the prodrugs was performed by comparing the integration of the doublet at 8 ppm, corresponding to 2 aromatic protons from one of the Ptx aromatic groups (noted 3 and 7 in Supplementary

1  
2  
3 Information, Figure S1) and the integration of the broad peak between 1.29 and 1.80 ppm  
4 corresponding to methylene protons of AAm repeat units.  
5  
6

7 *Size exclusion chromatography (SEC).* SEC was performed on a set-up from Viscotek  
8 (TDAmx) composed of a TDA 305 Triple Detector Array containing a differential viscometer,  
9 a right-angle laser-light scattering (90°, RALLS) detector, low-angle laser-light scattering (7°,  
10 LALLS) detector and refractive index (RI) detector. The chromatographic column set consisted  
11 of a guard column (PL, 50 × 7.5 mm) followed by two columns (PSS Gram, 300 × 8 mm; bead  
12 diameter 10 μm; molar mass range 500–10<sup>6</sup> g.mol<sup>-1</sup>). The system was equipped with a triple  
13 detection system (Viscotek TDA/GPCmax from Malvern) comprising a differential refractive  
14 index detector, low and right-angle light scattering detectors, a differential viscometer detector  
15 and a UV detector. The GPCmax was composed of an on-line degasser and a dual piston pump  
16 set at a flow rate of 0.7 mL.min<sup>-1</sup> with DMSO as the eluent, previously filtered through a 0.2  
17 μm filter. The TDAmx was thermostated at 50°C. The system was calibrated using a narrow  
18 pullulan standard and each polymer sample was injected at 5 different injection volumes to  
19 determine the refractive index increment ( $dn/dc = 0.057 \text{ mL.g}^{-1}$ ). Before the injection (100 μL),  
20 the samples were filtered through a polytetrafluoroethylene (PTFE) membrane with 0.2 μm  
21 pore. This allowed the molar mass ( $M_{n,SEC}$ ) and the dispersity ( $D = M_w/M_n$ ) of the polymers to  
22 be determined by triple detection using the OmniSEC software version 4.6.1.354.  
23  
24  
25  
26  
27  
28  
29  
30  
31  
32  
33  
34  
35  
36  
37  
38  
39  
40  
41  
42  
43

44 *Rheological measurements.* All rheological measurements were carried out on a rotational  
45 rheometer ARG2 (TA instruments, New Castle, USA). The geometry was an aluminum  
46 plate/plate (diameter 20 mm) equipped with a solvent trap. The TRIOS software was used for  
47 data analysis. Flow properties of the prodrugs were determined at 20 °C by a stress sweep. After  
48 a 2-min equilibration time, the shear rate was increased gradually from 10 to 1000 s<sup>-1</sup>.  
49  
50  
51  
52  
53  
54

55 *Injectability.* Injectability tests were carried out using a custom-built device described  
56 previously.<sup>29</sup> This device was coupled to a texture analyzer TAXT2 (Stable MicroSystems,  
57  
58  
59  
60



1  
2  
3 Godalming, UK) in compression mode which was equipped with a force transducer calibrated  
4 with a 30 kg sensor. 400  $\mu$ L of solution are taken in a 1-mL syringe (MeritMedical, Medaillon®  
5 Syringe, USA) which is then fitted with a 26 G x ½'' needle (0.45  $\times$  12 mm, Terumo Neolus,  
6 Japan) before injection at a 1 mm.s<sup>-1</sup> rate.  
7  
8  
9  
10

11  
12 *Liquid chromatography-tandem mass spectrometry (LC-MS/MS)*. Liquid chromatography  
13 conditions were as follows: C<sub>18</sub> (HILIC) column (Nucleodur, EC 125/2, 100-5-C18, Macherey-  
14 Nagel, Hoerd, France). Mobile phase: acetonitrile/water (50/50) with formic acid 0.1 %; run  
15 time: 8 min; flow rate: 0.3 mL.mL<sup>-1</sup>. ESI-MS/MS Analyses were performed on a triple  
16 quadrupole mass spectrometer detector (TQD) with electrospray ionization (ESI) interface  
17 (Quattro Ultima, Waters, Guyancourt, France). Electrospray and mass parameters were  
18 optimized by direct infusion of pure analytes into the system. ESI parameters: capillary voltage  
19 3.5 kV, cone voltage 35 V, source temperature 120 °C desolvation temperature 350 °C, with a  
20 nitrogen flow of 506 L.h<sup>-1</sup>. Mass parameters: transitions were monitored as follows Ptx  
21 854/286; Ptx-d<sub>5</sub> 859/291. Calibration: Calibration curve was linear in the range 5–1000 ng.mL<sup>-1</sup>  
22 ( $y = 0.0047.x + 0.0838$ ;  $R^2 = 0.9936$  in PBS and  $y = 0.0052.x - 0.0131$ ;  $R^2 = 0.9949$  in mouse  
23 plasma).  
24  
25  
26  
27  
28  
29  
30  
31  
32  
33  
34  
35  
36  
37  
38  
39  
40  
41

## 42 **Synthesis**

43  
44 *Synthesis of Ptx-ester-CDSPA and [<sup>3</sup>H]-Ptx-ester-CDSPA*. CDSPA (121 mg, 0.30 mmol),  
45 DMAP (40 mg, 0.33 mmol) and EDC.HCl (67 mg, 0.35 mmol) were dissolved in 2 mL  
46 anhydrous CH<sub>2</sub>Cl<sub>2</sub> and mixed in a reaction flask under argon at room temperature. After 15  
47 min, a solution of Ptx (100 mg, 0.12 mmol) in DMF (0.5 mL) was added dropwise into the  
48 flask. After stirring at 30 °C for 4 h, an additional 20 mg (0.10 mmol) of EDC.HCl solution in  
49 200  $\mu$ L anhydrous dichloromethane (DCM) was added. The reaction was stirred at 30 °C for  
50 another 22 h and was poured into 20 mL of ethyl acetate (EtOAc). The organic phase was  
51  
52  
53  
54  
55  
56  
57  
58  
59  
60

1  
2  
3 washed with aqueous NaHCO<sub>3</sub> and brine before being dried over MgSO<sub>4</sub>. The residue was  
4  
5 concentrated under reduced pressure and purified by flash chromatography (SiO<sub>2</sub>, from  
6  
7 DCM/EtOAc = 5/1 to DCM/EtOAc = 4/1, v/v) to give 88 mg (0.071 mmol) of Ptx-*ester*-  
8  
9 CDSPA as a yellow, sticky solid. Yield = 61%. <sup>1</sup>H NMR (300 MHz, CDCl<sub>3</sub>): δ = 8.17 (d, *J* =  
10  
11 7.6 Hz, 2H), 7.78 (d, *J* = 7.5 Hz, 2H), 7.72 – 7.31 (m, 15H), 6.93 (d, *J* = 8.9 Hz, 1H), 6.54 –  
12  
13 6.15 (m, 2H), 6.01 (d, *J* = 8.9 Hz, 1H), 5.70 (d, *J* = 7.0 Hz, 1H), 5.51 (d, *J* = 3.2 Hz, 1H), 5.00  
14  
15 (d, *J* = 8.7 Hz, 1H), 4.47 (s, 1H), 4.28 (dd, *J* = 34.7, 8.5 Hz, 2H), 3.84 (d, *J* = 6.8 Hz, 1H), 3.34  
16  
17 (t, *J* = 9.4 Hz, 1H), 2.51 (d, *J* = 13.8 Hz, 6H), 2.25 (s, 3H), 1.96 (s, 2H), 1.83 (d, *J* = 3.1 Hz,  
18  
19 3H), 1.78 – 1.60 (m, 10H), 1.38 – 1.13 (m, 20H), 0.90 (t, *J* = 6.5 Hz, 3H). <sup>13</sup>C NMR (75 MHz,  
20  
21 CDCl<sub>3</sub>): δ = 216.8, 203.8, 171.2, 170.7, 169.8, 167.9, 167.0, 142.6, 136.8, 133.7, 133.5, 132.9,  
22  
23 132.0, 130.2, 129.2, 128.7, 128.6, 127.2, 126.5, 119.0, 84.5, 81.1, 79.1, 76.4, 75.6, 75.1, 74.7,  
24  
25 72.1, 72.0, 58.5, 52.8, 46.3, 45.6, 43.2, 37.1, 35.5, 33.6, 31.9, 29.6, 29.5, 29.4, 29.3, 29.1, 28.9,  
26  
27 27.7, 26.8, 24.8, 24.8, 22.7, 22.7, 22.1, 20.8, 14.8, 14.1, 9.6.

28  
29  
30  
31  
32  
33 For [<sup>3</sup>H]-Ptx-*ester*-CDSPA, the procedure was the same except that [<sup>3</sup>H]-Ptx was added  
34  
35 in the reaction mixture as follows. Ethanol was carefully evaporated under vacuum from the  
36  
37 initial stock solution of [<sup>3</sup>H]-Ptx. [<sup>3</sup>H]-Ptx (1 mCi) was then solubilized in 100 μL of DMF prior  
38  
39 to addition to the reaction mixture containing non-radiolabeled Ptx (100 mg, 0.12 mmol) and  
40  
41 the other reagents in 200 μL of DMF. The vial containing the initial [<sup>3</sup>H]-Ptx was further rinsed  
42  
43 twice with 100 μL of DMF and these volumes were added to the reaction mixture. The  
44  
45 following steps were identical to those described for the synthesis of Ptx-*ester*-CDSPA and a  
46  
47 mixture of Ptx-*ester*-CDSPA/[<sup>3</sup>H]-Ptx-*ester*-CDSPA with a total activity of 258 μCi was  
48  
49 obtained as a yellow sticky solid. Yield = 19 %.

50  
51  
52  
53  
54 *Synthesis of Ptx-carbonate-CDP*. To a solution of Ptx (194 mg, 0.227 mmol) in dry DCM (4  
55  
56 mL) under an argon atmosphere was added 4 drops of pyridine. Then 4-nitrophenyl  
57  
58 chloroformate (273 mg, 1.362 mmol) in dry DCM was added at -50 °C, the reaction mixture  
59  
60

1  
2  
3 was stirred at -50 °C and after 4 h, 4-nitrophenyl chloroformate (183 mg, 0.908 mmol) was  
4  
5 added again. After 1 h the mixture was diluted with DCM and washed with sodium bicarbonate  
6  
7 (NaHCO<sub>3</sub>, 0.5 N) and brine and dried over anhydrous sodium sulfate. The organic layer was  
8  
9 separated and evaporated under vacuum. After evaporation of the solvents the crude was  
10  
11 purified by column chromatography (ethyl acetate-cyclohexane, 1:1), to yield activated  
12  
13 paclitaxel. Yield 45 %. <sup>1</sup>H NMR (300 MHz, CDCl<sub>3</sub>): δ = 8.28 (d, *J* = 9.2 Hz, 2H), 8.18 (d, *J* =  
14  
15 7.2 Hz, 2H), 7.77 (d, *J* = 7.3 Hz, 2H), 7.69 – 7.32 (m, 13H), 6.91 (d, *J* = 9.4 Hz, 1H), 6.33 (d,  
16  
17 *J* = 15.5 Hz, 2H), 6.12 (d, *J* = 9.5 Hz, 1H), 5.72 (d, *J* = 7.0 Hz, 1H), 5.55 (d, *J* = 2.6 Hz, 1H),  
18  
19 4.99 (d, *J* = 8.0 Hz, 1H), 4.54 – 4.40 (m, 1H), 4.35 (d, *J* = 8.3 Hz, 1H), 4.23 (d, *J* = 8.4 Hz, 1H),  
20  
21 3.84 (d, *J* = 7.0 Hz, 1H), 2.55 – 2.40 (m, 4H), 2.34 – 2.17 (m, 4H), 1.95 (s, 3H), 1.89 (d, *J* =  
22  
23 16.7 Hz, 1H), 1.81 (s, 1H), 1.71 (s, 3H), 1.67 (s, 2H), 1.28 (s, 3H), 1.17 (s, 3H). <sup>13</sup>C NMR (75  
24  
25 MHz, CDCl<sub>3</sub>): δ = 203.7, 171.2, 169.8, 167.3, 167.1, 154.9, 151.7, 142.3, 136.3, 133.7, 133.3,  
26  
27 133.1, 132.2, 130.2, 129.3, 129.2, 128.8, 128.8, 127.1, 126.5, 125.4, 121.6, 84.4, 81.2, 79.2,  
28  
29 75.5, 72.5, 72.1, 58.5, 52.6, 45.6, 43.2, 35.6, 26.9, 22.8, 22.2, 20.8, 14.8, 9.6.

30  
31  
32  
33  
34  
35 Activated Ptx (220 mg, 0.215 mmol) and CDP (83 mg, 0.215 mmol) in dry DCM (12  
36  
37 mL) were treated at room temperature with DMAP (31 mg, 0.258 mmol). The reaction mixture  
38  
39 was stirred in the dark for 48 h and was then diluted with DCM. The organic layer was washed  
40  
41 with saturated NaHCO<sub>3</sub> and dried over anhydrous sodium sulfate. The organic layers were  
42  
43 concentrated and the crude was purified with column chromatography using cyclohexane/ethyl  
44  
45 acetate as eluant (using a gradient from 80/20 to 50/50). The compound was isolated as yellow  
46  
47 powder. Yield 74 %. <sup>1</sup>H NMR (300 MHz, CDCl<sub>3</sub>): δ = 8.17 (d, *J* = 7.3 Hz, 2H), 7.78 (d, *J* = 8.0  
48  
49 Hz, 2H), 7.68 – 7.34 (m, 11H), 6.95 (d, *J* = 9.1 Hz, 1H), 6.32 (s, 2H), 6.02 (d, *J* = 8.5 Hz, 1H),  
50  
51 5.71 (d, *J* = 7.1 Hz, 1H), 5.44 (s, 1H), 5.00 (d, *J* = 8.7 Hz, 1H), 4.55 – 4.41 (m, 1H), 4.35 (d, *J*  
52  
53 = 8.6 Hz, 1H), 4.23 (d, *J* = 7.2 Hz, 3H), 3.84 (d, *J* = 7.5 Hz, 1H), 3.34 (t, *J* = 7.3 Hz, 2H), 2.58  
54  
55 – 2.37 (m, 5H), 2.22 (d, *J* = 19.3 Hz, 5H), 1.96 (s, 4H), 1.89 (s, 3H), 1.71 (s, 8 H), 1.48 – 1.12  
56  
57  
58  
59  
60

(m, 26H), 0.90 (t,  $J = 6.5$  Hz, 3H).  $^{13}\text{C}$  NMR (75 MHz,  $\text{CDCl}_3$ ):  $\delta = 203.8, 171.2, 169.9, 167.7, 167.0, 154.0, 142.6, 136.7, 133.7, 132.1, 130.2, 129.2, 128.7, 128.6, 127.2, 126.6, 84.5, 81.1, 79.2, 75.6, 75.1, 72.1, 67.8, 58.5, 57.7, 52.7, 47.2, 46.6, 45.6, 43.2, 37.1, 35.6, 29.6, 28.9, 27.7, 26.9, 24.9, 24.2, 22.7, 22.7, 22.2, 20.8, 14.8, 14.1$ . MS (ESI) $^+$ : 1291.7 ( $\text{M} + \text{Na}$ ) $^+$ .

*Synthesis of Ptx-ester-PAAm, Ptx-diglycolate-PAAm and Ptx-carbonate-PAAm.*

In a 7-mL glass vial were added AIBN (0.8 mg, 0.005 mmol), the Ptx-functionalized RAFT agents [Ptx-ester-CDSIPA (30 mg, 0.024 mmol, for **P3e**) or Ptx-diglycolate-CDP (30.18 mg, 0.022 mmol, for **P3d**) or Ptx-carbonate-CDP (30.18 mg, 0.024 mmol, for **P3c**)], AAm (454 mg, 6.39 mmol) and DMSO (1.6 mL). The mixture was degassed with argon for 15 min under vigorous stirring before being placed in a 70 °C-preheated oil bath for 24 h under stirring. After the reaction, the polymer was precipitated twice in methanol (MeOH). The polymer was further solubilized in DMSO and placed in a 3.5 kDa Spectra/Por 3 dialysis bag for dialysis against de-ionized water for 3 days, with dialysis water changed twice per day. The dialysate was then freeze-dried to yield Ptx-ester-PAAm (**P3e**), Ptx-diglycolate-PAAm (**P3d**) or Ptx-carbonate-PAAm (**P3c**), respectively, as a white-to-yellow, spongy solid. Another two polymerizations were carried out with  $[\text{AAm}]_0/[\text{PTX-ester-CDP}]_0 = 53$  (**P1e**) and 123 (**P2e**).

*Synthesis of [ $^3\text{H}$ ]-Ptx-ester-PAAm.* The radiolabeled [ $^3\text{H}$ ]-Ptx-ester-PAAm was obtained following the same procedure as for **P3e** except that the previously synthesized mixture of Ptx-ester-CDSIPA/ $^3\text{H}$ -Ptx-ester-CDSIPA was used as the RAFT agent and the purification only consisted in two precipitations in MeOH. The obtained polymer was thoroughly dried under vacuum before being dissolved directly in PBS. This solution was then mixed with a solution of non-radiolabeled Ptx-ester-PAAm **P3e** in PBS to the desired Ptx equivalent concentration and radioactivity for further in vivo studies.

*Multi-gram scale synthesis of Ptx-ester-PAAm.* Synthesis was performed as described previously with some modifications. Briefly, in a round bottom flask, CDSIPA $^+$  (3.86 g, 0.0095

1  
2  
3 mol), DMAP<sup>+</sup> (0.84 g, 0.0068 mol) and EDC.HCl<sup>+</sup> (1.78 g, 0.0093 mol) were dissolved in 20  
4 mL anhydrous CH<sub>2</sub>Cl<sub>2</sub> and 15 drops of anhydrous DMF (+these reagents were added portion-  
5 wise over 20 h), and mixed in a reaction flask under argon at room temperature. After 15 min,  
6 a solution of Ptx (4 g, 0.0046 mol) in DCM (20 mL) was added dropwise into the flask. After  
7 stirring at 30 °C for 29 h. The organic phase was washed with aqueous NaHCO<sub>3</sub> and brine  
8 before being dried over MgSO<sub>4</sub>. The residue was concentrated under reduced pressure and  
9 purified by flash chromatography (SiO<sub>2</sub>, from DCM-EtOAc 8:2) to give Ptx-*ester*-CDSPA as a  
10 yellow solid. Yield = 85%. In a 250 mL round bottom flask were added AIBN (36 mg, 0.2  
11 mmol), Ptx-*ester*-CDSPA (1.363 g, 1.089 mmol), AAm (2.613 g, 290 mmol) and DMSO (72.5  
12 mL). The mixture was degassed with argon for 15 min under vigorous stirring before being  
13 placed in a 70 °C-oil bath for 3 h under stirring. After the reaction, the polymer was precipitated  
14 twice in MeOH. The polymer was further solubilized in DMSO and placed in a 3.5 kDa  
15 Spectra/Por 3 dialysis bag for dialysis against de-ionized water for 5 days, with dialysis water  
16 changed twice per day. The dialysate was then freeze-dried to yield 14 g of Ptx-*ester*-PAAm  
17 ( $M_{n,NMR} = 24\ 000\ \text{g}\cdot\text{mol}^{-1}$ ,  $M_{n,SEC} = 24\ 780\ \text{g}\cdot\text{mol}^{-1}$ ,  $D = 1.17$ ) as a white-to-yellow spongy solid.  
18 Yield = 70 %.

19  
20  
21  
22  
23  
24  
25  
26  
27  
28  
29  
30  
31  
32  
33  
34  
35  
36  
37  
38  
39  
40  
41  
42  
43  
44  
45  
46  
47  
48  
49  
50  
51  
52  
53  
54  
55  
56  
57  
58  
59  
60  
*Determination of residual acrylamide.* Analyses were achieved by HPLC via isocratic runs  
(phosphate buffer mobile phase, 0.6 mL.min<sup>-1</sup> flow rate) on a RP-C18 column, 5 μm particle  
size (250 × 4.6 mm) and a guard column (5 × 3.9 mm) at a wavelength detection of 208 nm  
and a temperature of 40 °C. Run time was 10 min. Isocratic analyses were performed with a  
phosphate buffer mobile phase (0.84 g KH<sub>2</sub>PO<sub>4</sub> in 960 mL of H<sub>2</sub>O and 40 mL of MeOH).  
Concentrations of 0.1, 0.5, 1, 2, 10, 30, 50 and 100 μg.mL<sup>-1</sup> of AAm in deionized water were  
used to build the calibration curve. Each concentration was injected 4 times. Samples from **P3e**  
at 25, 50 and 100 mg.mL<sup>-1</sup> in deionized water were used to determine the residual amount of

1  
2  
3 AAm. Column washing between each run was performed by 1 wash with distilled-deionized  
4 water and 1 wash with MeOH.  
5  
6  
7  
8  
9

### 10 **In vitro evaluation**

11  
12 *Drug release.* Ptx release experiments were performed in PBS (1X, pH 7.4 with 1 wt.% Tween  
13 80) and in mouse plasma. Free Ptx, **P3e**, **P3d** and **P3c** (Table 1) were incubated in PBS and  
14 plasma at 37 °C at the same equivalent Ptx concentration (1  $\mu\text{g}\cdot\text{mL}^{-1}$  eq. Ptx). 200  $\mu\text{L}$  samples  
15 were taken at 0, 2, 4, 6, 24 and 48 h, for quantification. The samples were mixed with 600  $\mu\text{L}$   
16 of acetonitrile and 20  $\mu\text{L}$  of a solution of deuterated Ptx (Ptx- $d_5$ ) at 1  $\mu\text{g}\cdot\text{mL}^{-1}$  (internal standard).  
17 Samples were shaken during 15 min and centrifuged at 3000 g for 10 min before analysis by  
18 LC-MS/MS.  
19  
20  
21  
22  
23  
24  
25  
26  
27

28 *Cell culture and cytotoxicity.* The cytotoxicity of the different prodrugs was evaluated on two  
29 human breast cancer cell lines (MCF-7 and SK-BR-3), obtained from ATCC (USA). SK-BR-3  
30 cells were cultured in DMEM F-12 HAM supplemented with penicillin (50  $\text{U}\cdot\text{mL}^{-1}$ ),  
31 streptomycin (50  $\mu\text{g}\cdot\text{mL}^{-1}$ ), 20% heat inactivated FBS and 0.01  $\text{mg}\cdot\text{mL}^{-1}$  bovine insulin. MCF-7  
32 cells were grown in EMEM supplemented penicillin (50  $\text{U}\cdot\text{mL}^{-1}$ ), streptomycin (50  $\mu\text{g}\cdot\text{mL}^{-1}$ ),  
33 10% heat-inactivated FBS, 1% non-essential amino acids (NEAA) and 5  $\text{mL}$  glutamine. Both  
34 types of cells were maintained at 37 °C and 5%  $\text{CO}_2$  in a humidified atmosphere and were split  
35 twice weekly. The cell viability was evaluated using the 3-[4,5-dimethylthiazol-2-yl]-3,5-  
36 diphenyltetrazolium bromide (MTT) assay. Cells were seeded in 100  $\mu\text{L}$  of culture medium ( $8$   
37  $\times 10^3$  cells/well for SK-BR-3 cells and  $5 \times 10^3$  cells/well for MCF-7 cells) in 96 well plates  
38 (TPP, Switzerland) and pre-incubated for 24 h. 100  $\mu\text{L}$  of a serial dilution of prodrug solution  
39 was then added to the medium. After 72 h of incubation, 20  $\mu\text{L}$  of MTT solution (5  $\text{mg}\cdot\text{mL}^{-1}$  in  
40 PBS) was added to each well. After 4 h of incubation, the culture medium was gently aspirated  
41 and replaced by 200  $\mu\text{L}$  DMSO to dissolve the formazan crystals. The absorbance of the  
42  
43  
44  
45  
46  
47  
48  
49  
50  
51  
52  
53  
54  
55  
56  
57  
58  
59  
60

1  
2  
3 solubilized dye, which correlates with the number of living cells, was measured with a  
4  
5 microplate reader (LAB Systems Original Multiscan MS, Finland) at 570 nm. The percentage  
6  
7 of viable cells in each well was calculated as the absorbance ratio between prodrug-treated and  
8  
9 untreated control cells. Data was fitted to a Hill slope model with four parameters using  
10  
11 GraphPad Prism (version 8.0.2) to determine the  $IC_{50}$ . The different  $IC_{50}$  values were  
12  
13 determined using a one-way ANOVA test with GraphPad Prism (version 8.0.2).  
14  
15  
16  
17  
18

### 19 **In vivo evaluation**

20  
21 *Ethic protocols.* All animal experiments were conducted according to the European rules  
22  
23 (86/609/EEC and 2010/63/EU) and the Principles of Laboratory Animal Care and legislation in  
24  
25 force in France (Decree No. 2013-118 of February 1, 2013). Toxicity, pharmacokinetics and  
26  
27 biodistribution experiments obtained experimental approval from the Ethical Committee  
28  
29 C2EA-26 (Comité d'éthique en expérimentation animale de l'IRCIV, Authorization number  
30  
31 APAFIS#7756). In vivo efficacy experiments were performed by Oncodesign (Les Ulis,  
32  
33 France) as study N°190015 and was approved by the Institutional Animal Care and Use  
34  
35 Committee of Oncodesign (Oncomet) approved by French authorities (CNREEA agreement N°  
36  
37 91).  
38  
39  
40  
41

42 *Acute toxicity and histology.* Groups of 3 mice were injected subcutaneously at day 0 in the  
43  
44 inter-scapular region. The different groups are: (i) Taxol at 60 and 90  $mg.kg^{-1}$  (positive control);  
45  
46 (ii) PAAm at 700, 1400, 2100, 2800, 3500 and 4200  $mg.kg^{-1}$  (polymer alone, negative control);  
47  
48 (iii) Ptx-*ester*-PAAm **P3e** at 90, 120, 150 and 180  $mg.kg^{-1}$  eq. Ptx; (iv) Ptx-*carbonate*-PAAm  
49  
50 **P3c** at 90, 120, 150 and 180  $mg.kg^{-1}$  eq. Ptx and (v) Ptx-*diglycolate*-PAAm **P3d** at 90, 120, 150  
51  
52 and 180  $mg.kg^{-1}$  eq. Ptx. Taxol was also injected intravenously in the tail vein at 10, 20, 30 and  
53  
54 60  $mg.kg^{-1}$ . Visual toxicities at the injection site and body weight were monitored daily to  
55  
56 follow local and systemic toxicities. After 7 days, mice were euthanized by cervical dislocation  
57  
58  
59  
60

1  
2  
3 and injection site were removed and fixed in PFA 4% (overnight). They were then transfer in  
4 ethanol 70% for maximum 1 week before paraffin-embedding (System Logos One, Micro  
5 France). After paraffin embedding, 4 microns thick tissue sections were made using a  
6 microtome (Autosection, Sakura). The slides were then stained (Austostainer XL, Leica) by  
7 Hematoxylin-Eosine-Saffron (HES) histopathological examination. A semi-quantitative  
8 scoring system, ranging from 0 (no change) to 3 (marked change), was applied.  
9

10  
11  
12 *Pharmacokinetics of Ptx by mass spectrometry.* Seven-week old female BALB/c OlaHsd mice  
13 (~22 g; Envigo, France) were divided into four different groups: (i) Taxol injected intravenously  
14 (7 mg.kg<sup>-1</sup>); (ii) Ptx-*ester*-PAAm injected subcutaneously (7 mg.kg<sup>-1</sup> eq. Ptx); (iii) Ptx-  
15 *diglycolate*-PAAm injected subcutaneously (7 mg.kg<sup>-1</sup> eq. Ptx) and (iv) Ptx-*carbonate*-PAAm  
16 injected subcutaneously (7 mg.kg<sup>-1</sup> eq. Ptx). Each group was composed of 36 mice divided in  
17 9 different time points (0.25, 0.5, 1, 2, 4, 7, 24, 48 and 72 h) leading to 4 mice per group. At  
18 each endpoint, mice were euthanized with pentobarbital and blood was sampled by cardiac  
19 puncture before plasma was recovered by centrifugation (5 min; 3000 g). After centrifugation,  
20 sample was prepared following the protocol bellow. Aliquots of 200 µL were mixed with 600  
21 µL of acetonitrile and 20 µL of deuterated Paclitaxel (Ptx-*d*<sub>5</sub>) at 1 µg.mL<sup>-1</sup> (internal standard).  
22 Samples were shaken during 15 min and centrifuged for 10 min before analysis by LC-MS/MS.  
23

24  
25  
26 *Pharmacokinetics and biodistribution of radiolabeled Ptx.* Seven-week old female  
27 BALB/cOlaHsd mice (~22 g; Envigo, France) were used. Radiolabeled Taxol and radiolabeled  
28 [<sup>3</sup>H]-Ptx-*ester*-PAAm were injected at 7 mg.kg<sup>-1</sup> equiv. Ptx (0.93 µCi per mouse) to perform  
29 the pharmacokinetics and the biodistribution. Mice were divided into four groups: (i) Taxol  
30 injected intravenously; (ii) Taxol® injected subcutaneously; (iii) [<sup>3</sup>H]-Ptx-*ester*-PAAm injected  
31 intravenously and (iv) [<sup>3</sup>H]-Ptx-*ester*-PAAm injected subcutaneously. Each group was  
32 composed of 40 mice divided in 10 different time points (0.25, 0.5, 1, 2, 4, 7, 24, 48, 96 and  
33 144 h) leading to 4 mice per group. At each endpoint, mice were euthanized with pentobarbital  
34  
35  
36  
37  
38  
39  
40  
41  
42  
43  
44  
45  
46  
47  
48  
49  
50  
51  
52  
53  
54  
55  
56  
57  
58  
59  
60



1  
2  
3 and blood was sampled by cardiac puncture before plasma was recovered by centrifugation (5  
4 min at 3000 g). Livers, kidneys, spleens, lungs and some SC tissue at the injection site were  
5 also collected. All samples were stored in a freezer (-20 °C) before analysis. For radioactivity-  
6 counting, approximately 100  $\mu$ L of plasma and 100 mg of each organ/tissue were taken and  
7 precisely weighted. Organs were first dissolved by adding 1 mL of solvable (PerkinElmer,  
8 USA) and samples were put in an oven at 60 °C overnight. They were then whitewashed by  
9 adding twice 100  $\mu$ L of H<sub>2</sub>O<sub>2</sub> 30% (w/v) and warmed for 30 min at 60 °C in an oven. Finally,  
10 plasma and treated organ samples were mixed with Ultimagold (PerkinElmer, USA) and  
11 radioactivity was measured with a LS 6500 multi-purpose scintillation counter (Beckman  
12 Coulter). Radioactive counting allowed access to total Ptx concentration and metabolites: [Total  
13 Ptx] = [Free Ptx] + [Ptx-*ester*-PAAm] + [Ptx metabolites]. Pharmacokinetic parameters were  
14 determined using PKSolver.<sup>30</sup>

15  
16  
17  
18  
19  
20  
21  
22  
23  
24  
25  
26  
27  
28  
29  
30  
31 *Anticancer efficacy.* 52 healthy female BALB/c nude mice, 6-8 weeks old were obtained from  
32 Charles River. After 2 weeks of acclimation, MCF-7 breast tumors were induced by  
33 subcutaneous injection of  $10 \times 10^6$  MCF-7 cells in 200  $\mu$ L RPMI 1640 medium into the right  
34 flank of mice. At day 17, when tumors reach a mean volume of 100–150 mm<sup>3</sup>, 40 animals out  
35 of 52 were randomized into 4 groups 9 animals each. Homogeneity of the mean tumor volume  
36 between groups was tested by an analysis of variance (ANOVA). The treatments started the  
37 day of randomization. Treatment was administered either by SC injection in the inter-scapular  
38 region or by IV injection into the caudal vein. A Q7Dx3 treatment schedule was applied as  
39 follows: (i) PAAm SC at 1520 mg.kg<sup>-1</sup>, once a week for 3 consecutive times (negative control);  
40 (ii) Ptx-*ester*-PAAm SC at 15 mg.kg<sup>-1</sup> (Taxol equivalent dose); (iii) Ptx-*ester*-PAAm SC at 60  
41 mg.kg<sup>-1</sup> (Taxol equivalent dose) which corresponds to Ptx-PAAm maximal tolerated dose and  
42 (iv) Taxol IV at 15 mg.kg<sup>-1</sup> (Taxol maximal tolerated dose). Animal viability and behavior were  
43 observed daily, and body weights were measured twice a week. Tumor volume was measured  
44  
45  
46  
47  
48  
49  
50  
51  
52  
53  
54  
55  
56  
57  
58  
59  
60

1  
2  
3 twice a week with a caliper and estimated with the following formula: Volume = (length ×  
4 width<sup>2</sup>) / 2. Mice were euthanized by overdosage on gas anesthesia (isoflurane) followed by  
5  
6 cervical dislocation when Humane endpoints were reached.<sup>31-32</sup>  
7  
8

9  
10 *Statistics.* Statistics were performed using GraphPad Prism (version 8.0.2). Comparison of  
11 tumor growth results between groups were analyzed for statistical significance, using two-way  
12 ANOVA, with Tukey multiple comparisons post-hoc.  
13  
14  
15  
16  
17  
18  
19  
20

## 21 **Results and Discussion**

### 22 **Synthesis and characterization**

23  
24  
25  
26  
27 The polymer prodrugs were synthesized by the “drug-initiated” method,<sup>33</sup> which relies on the  
28 controlled growth of a polymer chain from a drug derivatized by a polymerization  
29 initiator/controlling agent to perform controlled polymerization. This strategy has been selected  
30 to facilitate clinical translation because of its simplicity and scalability, since only a few high-  
31 yielding synthesis steps are necessary. It is also very robust and flexible since it is easily  
32 applicable to different drugs/linkers/polymers,<sup>28, 34-37</sup> leading to a broad range of different  
33 polymer prodrugs with tunable drug delivery properties.  
34  
35  
36  
37  
38  
39  
40  
41  
42

43 A small library of well-defined Ptx-PAAm prodrugs was synthesized by reversible  
44 addition-fragmentation chain transfer (RAFT) polymerization of AAm using Ptx-based,  
45 trithiocarbonate chain transfer agents (Figures 2 and S1). Three different linkers were  
46 investigated (ester, carbonate and diglycolate) to find the optimal balance in terms of linker  
47 stability vs. lability to prevent early drug release into the SC tissue, while ensuring its release  
48 into the blood before prodrug excretion (Figure 1b and 2). These linkers were chosen for their  
49 sensitivity to circulating enzymes with esterase activity and with moderate expression  
50 variability in humans, thus ensuring comparable interpatient drug release patterns.<sup>38-39</sup>  
51  
52  
53  
54  
55  
56  
57  
58  
59  
60

Ptx-*ester*-PAAm was obtained by coupling Ptx to CDSPA as a chain transfer agent (Figures 2 and S1a), followed by RAFT polymerization at 70°C in DMSO using AIBN as initiator (Figures 2 and S2). By adjusting the  $[AAm]_0/[Ptx\text{-}ester\text{-}CDSPA]_0$  ratio from 53 to 266, the PAAm chain length was varied to determine the minimal  $M_n$  that allows for complete solubilization of the prodrug in water, which is a prerequisite to prevent SC toxicity and warrant high SC bioavailability.  $^1H$  NMR spectroscopy of the purified prodrugs showed all expected signals, especially amide, methylene and methine protons from the PAAm backbone together with aromatic and characteristic protons from Ptx (Figure S2).

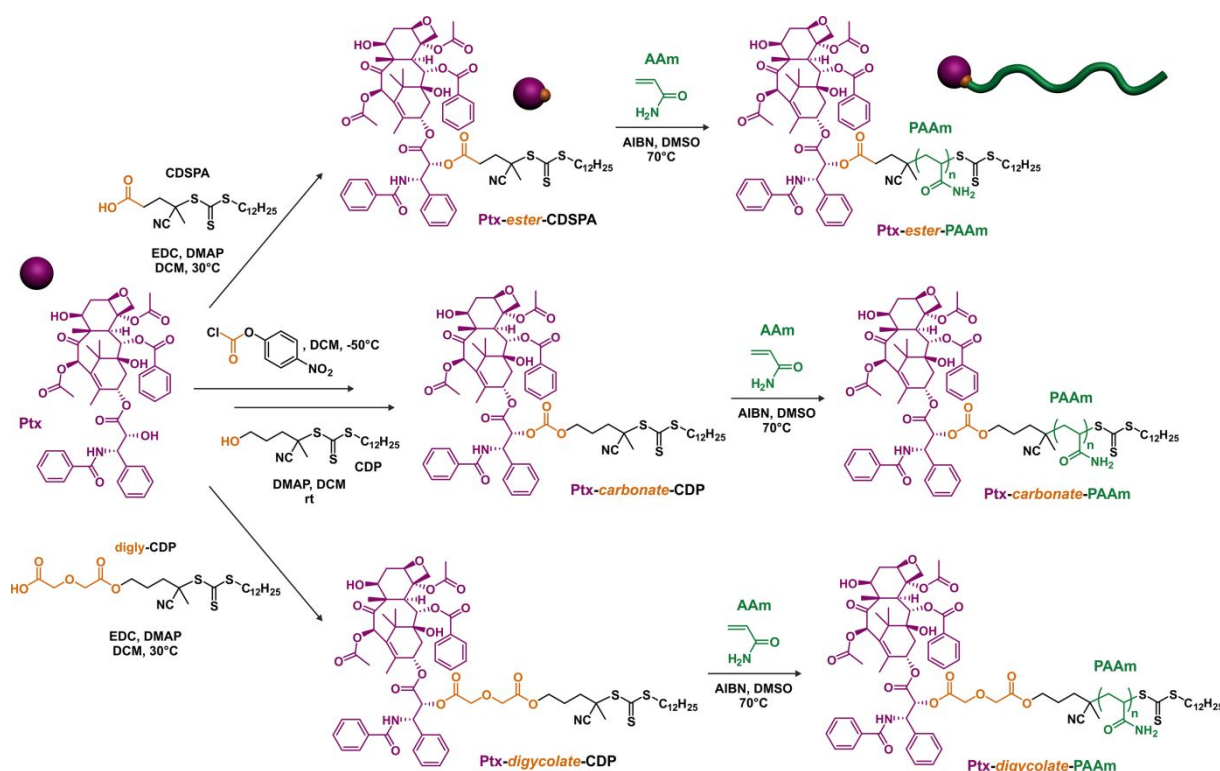


**Figure 2.** Synthesis of water-soluble, paclitaxel-polyacrylamide (Ptx-PAAm) prodrugs with ester, carbonate or diglycolate linker by RAFT polymerization of acrylamide (AAm) from Ptx-*ester*-CDSPA, Ptx-*carbonate*-CDP or Ptx-*diglycolate*-CDP RAFT agent, respectively.

The prodrugs exhibited  $M_{n,NMR}$  ranging from 6 200 to 21 600  $g \cdot mol^{-1}$  in rather good agreement with  $M_{n,SEC}$  values (**P1e–P3e**, Table 1 and Figure S3) and low dispersities ( $D = 1.07–1.28$ ), thus accounting for a controlled polymerization process. By tuning the PAAm chain length, the drug

loading varied from ~14 to ~4 wt.%. Whereas **P1e** and **P2e** were only partially soluble in water at 3 mg.mL<sup>-1</sup> eq. Ptx because of the too short PAAm chains, **P3e** ( $M_{n,NMR} = 21\ 600\ \text{g.mol}^{-1}$ ) was fully water-soluble at this equiv. Ptx concentration, which represents a 104-fold increase in solubility compared with free Ptx.

**Table 1.** Macromolecular characteristics and solubility of the different Ptx-PAAm polymer prodrugs synthesized in this study.

Sample	Linker	$M_{n,NMR}$ (g.mol <sup>-1</sup> )	$M_{n,SEC}^a$ (g.mol <sup>-1</sup> )	$D^a$	%Ptx <sup>b</sup> (wt.%)	Solubility <sup>c</sup>
<b>P1e</b>	Ester	6 200	9 100	1.07	13.8	Insoluble
<b>P2e</b>	Ester	9 400	15 200	1.28	9.1	Insoluble
<b>P3e</b>	Ester	21 600	29 100	1.12	4.0	Soluble
<b>P3d</b>	Digly	27 300	36 000	1.10	3.1	Soluble
<b>P3c</b>	Carbonate	23 000	39 900	1.09	3.7	Soluble

<sup>a</sup> Determined by triple detection SEC. <sup>b</sup> Calculated by  $M_{n,NMR}$ . <sup>c</sup> Solubility tests were performed in water at a Ptx equivalent concentration of 3 mg.mL<sup>-1</sup> to assess the presence of insoluble aggregates or not.

The structure of the RAFT agent was then modified to change the nature of the linker. Previous reports have shown that diglycolate-based linkers are highly labile in plasma with faster release kinetics than the ester counterparts,<sup>28, 36, 40</sup> whereas carbonate linkers have shown slower release kinetics.<sup>41</sup> Therefore, well-defined Ptx-carbonate-PAAm (**P3c**) and Ptx-diglycolate-PAAm (**P3d**) of similar  $M_n$  to that of **P3e** were synthesized (Figures S1–S3, Table 1). They were obtained by following an identical polymerization procedure to that of the Ptx-carbonate-CDP and Ptx-diglycolate-CDP functional RAFT agents, respectively (Figure 2). Those were synthesized by activation of Ptx by 4-nitrophenyl chloroformate followed by reaction with CDP, or by coupling Ptx to diglycolate-CDP.

Successful clinical translation requires simple and robust manufacturing methods that ensure the preparation of newly developed materials in large scales and with a high level of purity.<sup>42</sup> In this context, we also performed a multi-gram scale synthesis of **P3e** where 4.8 g of

Ptx-*ester*-CDSPA and 17.6 g of the corresponding polymer prodrug ( $M_{n,NMR} = 24\ 000\ \text{g}\cdot\text{mol}^{-1}$ ,  $M_{n,SEC} = 24\ 780\ \text{g}\cdot\text{mol}^{-1}$ ,  $D = 1.17$ ) were obtained, with an overall yield of 60%. The high purity of **P3e** was assessed by HPLC, leading to residual amounts of free AAm and Ptx both below 1 ppm, much lower than the average dietary intake of AAm ( $1\ \mu\text{g}\cdot\text{kg}^{-1}\ \text{body weight}\cdot\text{day}^{-1}$ )<sup>43</sup> and below the threshold established by the European Medicines Agency for AAm in cosmetics.<sup>44</sup>

### Physicochemical characteristics and in vitro evaluation

Prior to performing biological evaluations, key physico-chemical characteristics were investigated: (i) the viscosity and injectability of the prodrugs in aqueous solution, to ensure they can be injected under standard conditions used for SC administration and (ii) the release kinetics of Ptx from the prodrugs in different media, to assess its fine tuning depending on the prodrug's structure.

Measuring the viscosity and injectability (i.e., force required for injection) of the prodrugs in aqueous solution is of crucial importance as the maximum volume generally accepted for a SC injection is  $\sim 2\ \text{mL}$ , thus requiring administration of the relatively concentrated solutions to reach the same dose regimens as the IV-administered counterparts. Whereas the viscosity of PAAm ( $M_{n,SEC} = 37\ 000\ \text{g}\cdot\text{mol}^{-1}$ ,  $D = 1.10$ ) synthesized by the same procedure was close to that of water ( $< 10\ \text{cP}$ ) at  $50\ \text{mg}\cdot\text{mL}^{-1}$ , viscosity of **P3e** was  $\sim 200\ \text{cP}$  at  $50\ \text{mg}\cdot\text{mL}^{-1}$  and increased to  $\sim 1 \times 10^4\ \text{cP}$  at  $200\ \text{mg}\cdot\text{mL}^{-1}$  (Figure S4). This is due to the presence of strongly hydrophobic Ptx moieties that induce the formation of hydrophobic domains, via Ptx-Ptx and likely Ptx-C<sub>12</sub> alkyl interactions, decreasing the mobility of the polymer chains.

The injectability of aqueous solutions of **P3e**, **P3d** and **P3c** was measured as the function of the concentration with a  $26\ \text{G} \times \frac{1}{2}$ " needle, as the preferred needle size for humans is  $\sim 25$ - $27\ \text{G}$ . Up to  $50\ \text{mg}\cdot\text{mL}^{-1}$ , injection of the polymer prodrugs required a very low force of  $\sim 1\ \text{N}$ ,

1  
2  
3 which was comparable to that of PAAm (Figure S5). Despite an increase in viscosity with the  
4  
5 polymer prodrug concentrations, a concentration as high as  $\sim 130 \text{ mg.mL}^{-1}$  was achieved  
6  
7 (corresponding to  $\sim 6 \text{ mg.mL}^{-1}$  in Ptx) at 30 N, which is the maximum acceptable injection force  
8  
9 for SC administration.<sup>45</sup>  
10

11  
12 The release of Ptx from the prodrugs **P3c**, **P3d** and **P3e** was then monitored in PBS and  
13  
14 in murine plasma at 37 °C to investigate the influence of both the nature of the linker and of the  
15  
16 medium (i.e., hydrolytic vs. hydrolytic + enzymatic cleavage) on the release kinetics. The  
17  
18 diglycolate moiety of **P3d** showed a dual hydrolytic/enzymatic susceptibility resulting in the  
19  
20 fastest release of Ptx in both media ( $\sim 50\%$  in PBS after 20 h and  $\sim 90\%$  in plasma after 5 h)  
21  
22 (Figure 3a and 3b). By comparison, **P3e** and **P3c** were both stable in PBS up to at least 70 h  
23  
24 and gave comparable Ptx release kinetics in plasma ( $\sim 40\%$  after 24 h). Release kinetics were  
25  
26 not monitored beyond 24 h in plasma due to the documented degradation of Ptx under these  
27  
28 conditions.<sup>46-47</sup>  
29  
30  
31  
32  
33  
34  
35  
36  
37  
38  
39  
40  
41  
42  
43  
44  
45  
46  
47  
48  
49  
50  
51  
52  
53  
54  
55  
56  
57  
58  
59  
60

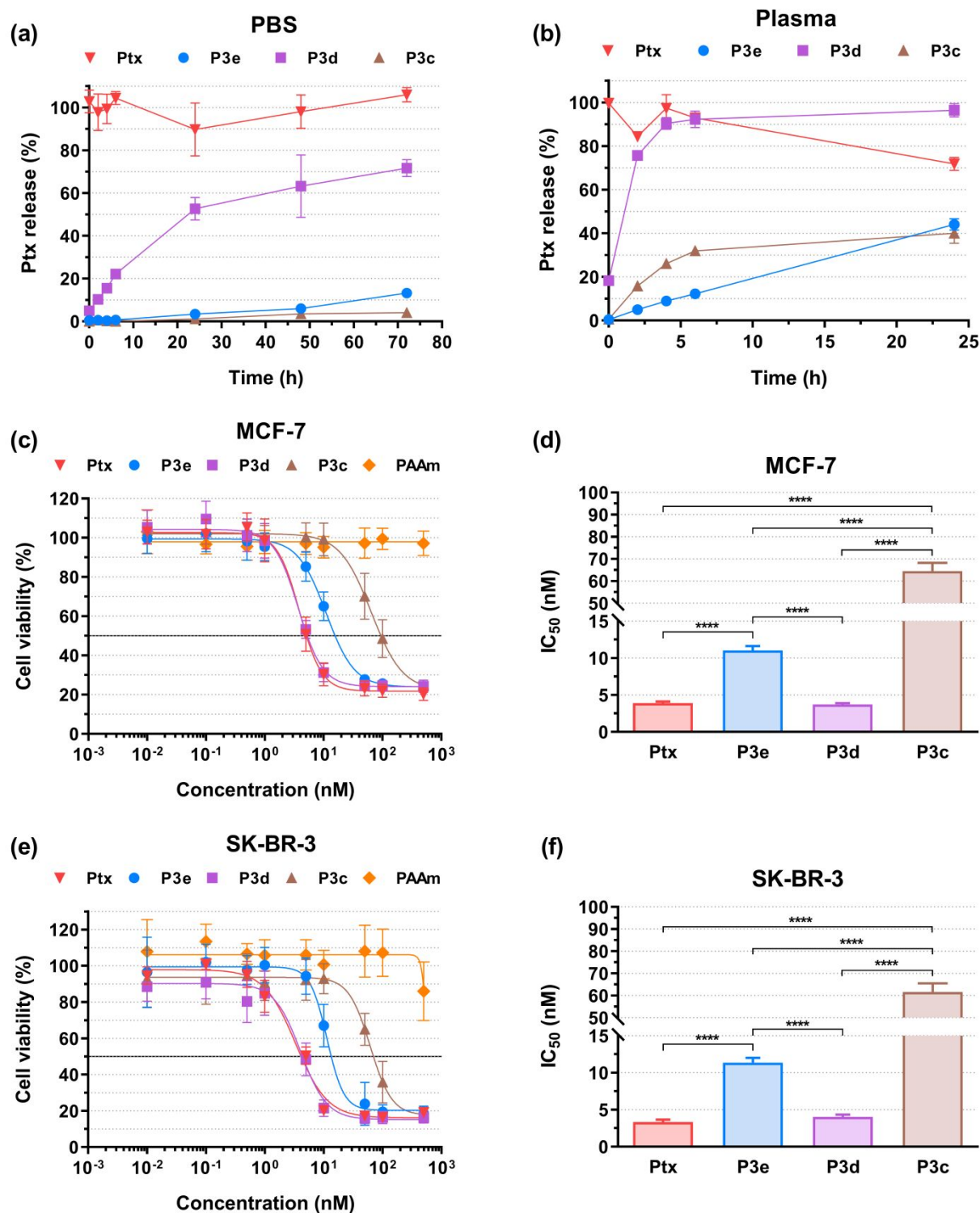


**Figure 3.** Ptx release profiles from **P3e**, **P3d** and **P3d** (Ptx is plotted as the reference) in: (a) PBS at 37°C and (b) murine plasma at 37°C. Cell viability (MTT test) with increasing concentrations of Ptx, **P3e**, **P3d**, **P3d** and PAAm on: (c) MCF-7 cells with (d) the corresponding IC<sub>50</sub>, and (e) SK-BR-3 cells with (f) the corresponding IC<sub>50</sub> values. The values are expressed as the means ± SD. Unpaired two-tailed *t* test; \*\*\*\* (*p* < 0.0001).

1  
2  
3 To assess whether the drug release profiles observed in plasma correlate with the cytotoxicity  
4 of the prodrugs, cell viability experiments were performed by measuring the mitochondrial  
5 activity via MTT assay on two breast cancer cell lines (MCF-7 and SK-BR-3), corresponding  
6 to clinically relevant cancer models for Ptx. Importantly, all prodrugs led to significant  
7 cytotoxicity on both cell lines and their  $IC_{50}$  values were in the following order: **P3d** < **P3e** <  
8 **P3c**. While PAAm was not cytotoxic (> 75% cell viability) up to 500 nM on both cell lines,  
9 free Ptx gave an  $IC_{50}$  as low as 5 nM (Figure 3c-3f). Since Ptx must be released from the prodrug  
10 before passively diffusing through the cell membranes to reach the microtubules, slow release  
11 in plasma might be correlated with a high  $IC_{50}$ . It is also interesting to note that: (i) due to the  
12 high lability of the diglycolate linker, **P3d** has the same  $IC_{50}$  as that of free Ptx and (ii) despite  
13 similar drug release profiles for **P3c** and **P3e** in PBS and plasma, **P3e** led to much lower  $IC_{50}$   
14 than that **P3c**, possibly due to differences in the enzymatic composition of murine plasma and  
15 cell culture medium.  
16  
17  
18  
19  
20  
21  
22  
23  
24  
25  
26  
27  
28  
29  
30  
31

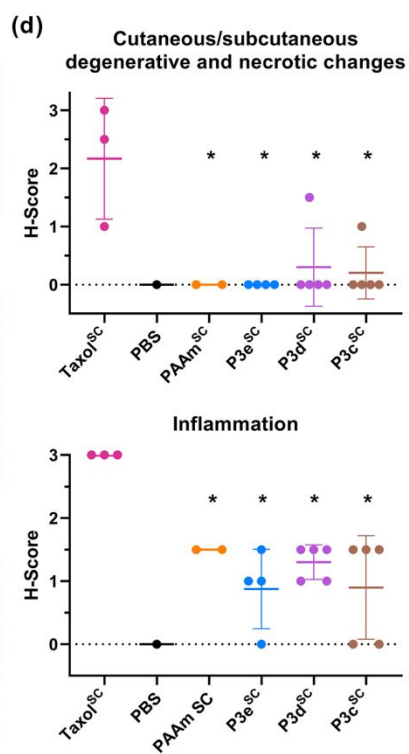
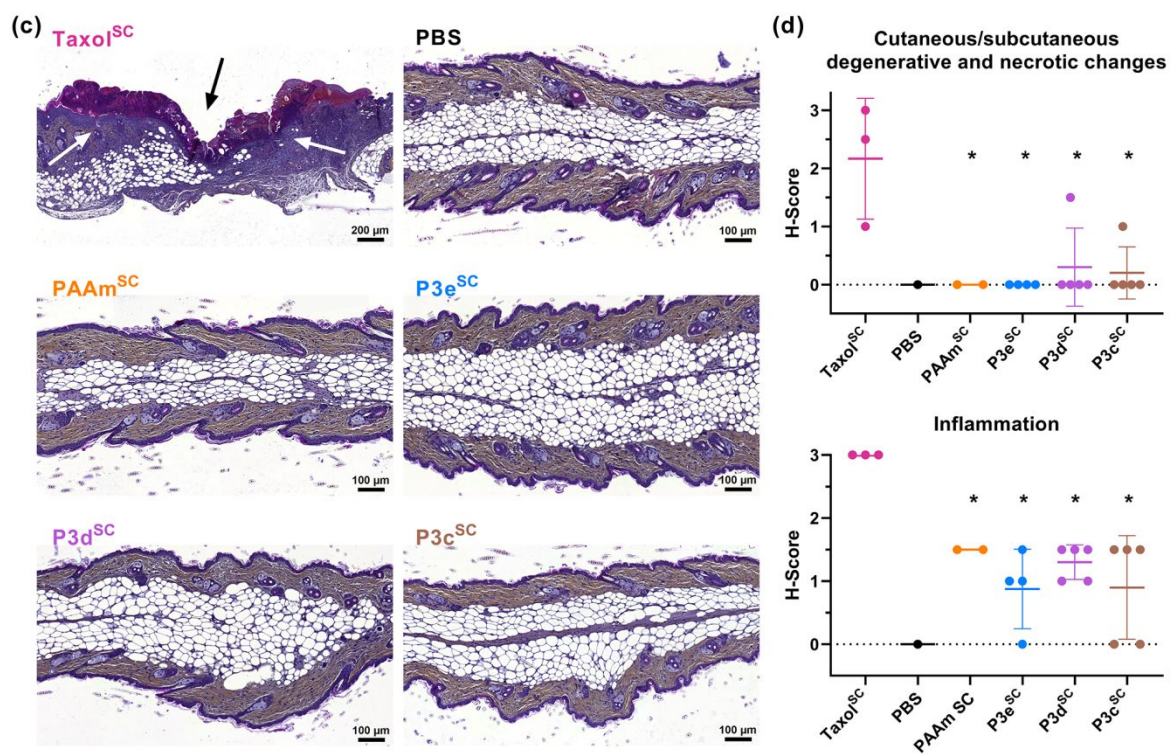
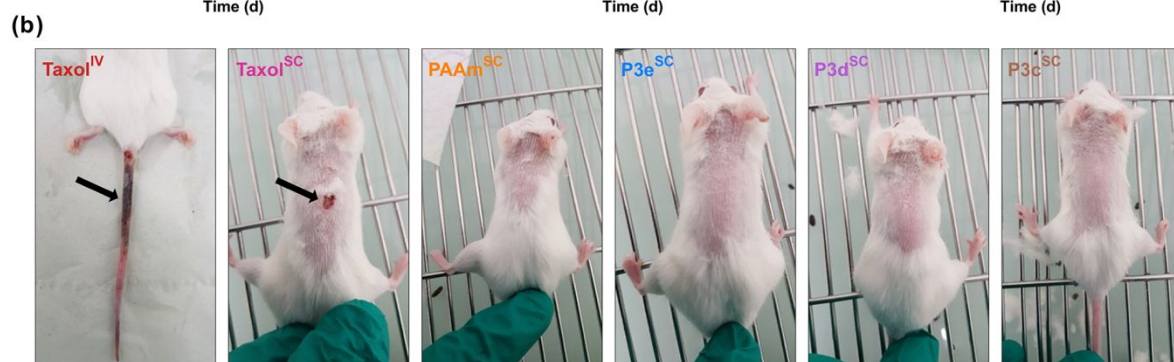
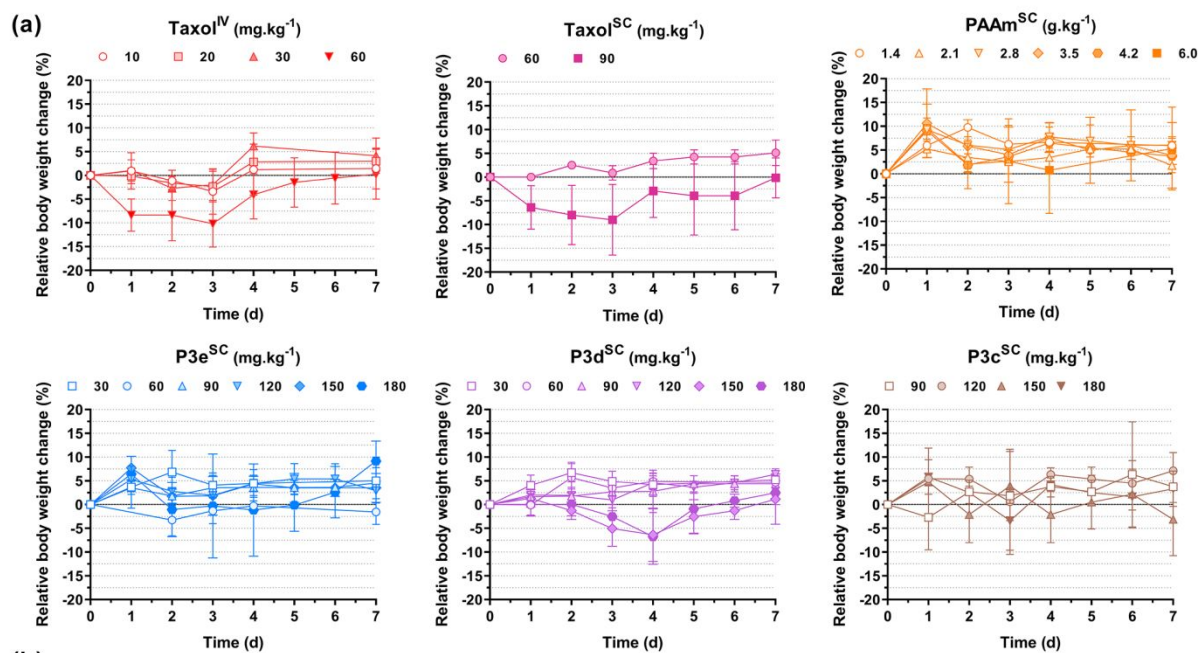
### 32 33 34 35 **Systemic and acute local toxicity**

36  
37 The systemic toxicity of the prodrugs was then examined in mice to evaluate the MTD (i.e. the  
38 threshold at which all animals survived with a body weight loss lower than 10%) to find  
39 optimized treatments, followed by evaluation of the acute local toxicity at the injection site  
40 (Figure 4).  
41  
42  
43  
44  
45

46  
47 Increasing concentrations of free PAAm and prodrugs **P3e**, **P3d** and **P3c** were SC  
48 injected (PAAm<sup>SC</sup>, **P3e**<sup>SC</sup>, **P3d**<sup>SC</sup> and **P3c**<sup>SC</sup>, respectively) to healthy mice (single injection),  
49 followed by monitoring of their body weight and their behavior for 7 days (Figure 4a). The  
50 same protocol was applied to SC and IV injections of Taxol (Taxol<sup>SC</sup> and Taxol<sup>IV</sup>, respectively).  
51 Whereas Taxol<sup>IV</sup> led to a MTD of 60 mg.kg<sup>-1</sup>, Taxol<sup>SC</sup> allowed to reach 90 mg.kg<sup>-1</sup>, probably  
52 due to a decrease in  $C_{max}$  compared with IV administration and thus a dose-limiting reduction  
53  
54  
55  
56  
57  
58  
59  
60



1  
2  
3 in  $C_{\max}$ -related.<sup>48</sup> Mice treated with free PAAm<sup>SC</sup> showed no sign of systemic toxicity up to a  
4 concentration as high as 6000 mg.kg<sup>-1</sup>, in good agreement with its well-documented  
5 biocompatibility/safety. Importantly, all prodrugs were successfully SC injected up to at least  
6 180 mg.kg<sup>-1</sup> equiv. Ptx without exceeding a body weight loss of 10%. Neither mortality nor  
7 noticeable modification in terms of feeding and behavior were observed, thus suggesting  
8 absence of systemic toxicity. Notably, the MTD was increased at least by a factor 3 and 2  
9 compared to Taxol<sup>IV</sup> and Taxol<sup>SC</sup>, respectively.  
10  
11  
12  
13  
14  
15  
16  
17  
18  
19  
20  
21  
22  
23  
24  
25  
26  
27  
28  
29  
30  
31  
32  
33  
34  
35  
36  
37  
38  
39  
40  
41  
42  
43  
44  
45  
46  
47  
48  
49  
50  
51  
52  
53  
54  
55  
56  
57  
58  
59  
60



1  
2  
3 **Figure 4.** (a) Relative body weight change of mice as a function of time after IV injection of Taxol  
4 (Taxol<sup>IV</sup>) and SC injection of Taxol (Taxol<sup>SC</sup>), PAAm (PAAm<sup>SC</sup>), **P3e** (**P3e<sup>SC</sup>**), **P3d** (**P3d<sup>SC</sup>**) and **P3c**  
5 (**P3c<sup>SC</sup>**). The values are expressed as the means  $\pm$  SD ( $n = 3$ ). (b) Representative pictures of mice ( $n =$   
6 3) 7 days after injection of Taxol<sup>IV</sup> at 60 mg.kg<sup>-1</sup>, Taxol<sup>SC</sup> at 60 mg.kg<sup>-1</sup>, PAAm<sup>SC</sup> at 4.2 g.kg<sup>-1</sup>, and  
7 **P3e<sup>SC</sup>**, **P3d<sup>SC</sup>** and **P3c<sup>SC</sup>** at 180 mg.kg<sup>-1</sup> (equiv. Ptx). The black arrows indicate necrotic areas. (c)  
8 Representative HES-stained sections of skin samples from mice removed at the injection site after  
9 injection of Taxol<sup>SC</sup> at 90 mg.kg<sup>-1</sup>, PBS, PAAm<sup>SC</sup> at 4.2 g.kg<sup>-1</sup>, and **P3e<sup>SC</sup>**, **P3d<sup>SC</sup>** and **P3c<sup>SC</sup>** at 180  
10 mg.kg<sup>-1</sup> (equiv. Ptx). The black/white arrows indicate the severe cutaneous necrosis, only observed after  
11 SC injection of Taxol at 90 mg.kg<sup>-1</sup>. (d) Histopathological scoring (H-Score) of degenerative/necrotic  
12 changes and tissular inflammation in mice after injection of Taxol<sup>SC</sup> at 90 mg.kg<sup>-1</sup>, PAAm<sup>SC</sup> up to 4.2  
13 g.kg<sup>-1</sup>, and **P3e<sup>SC</sup>**, **P3d<sup>SC</sup>** and **P3c<sup>SC</sup>** up to 180 mg.kg<sup>-1</sup> (equiv. Ptx). The values are expressed as the  
14 means  $\pm$  SD. Unpaired two-tailed  $t$  test between Taxol<sup>SC</sup> group and PAAm<sup>SC</sup>, **P3e<sup>SC</sup>**, **P3d<sup>SC</sup>** or **P3c<sup>SC</sup>**  
15 group; \* ( $p < 0.05$ ). See all pictures and individual scores in Figure S6 and Table S1.

16  
17  
18  
19  
20  
21  
22  
23  
24  
25  
26 Similarly to free PAAm<sup>SC</sup>, none of the prodrugs showed local toxicity at and near the injection  
27 site up to 180 mg.kg<sup>-1</sup> equiv. Ptx (Figure 4b). This observation likely ruled out early Ptx release  
28 in the SC tissue from the prodrugs even from **P3d<sup>SC</sup>** that contains the most labile linker.  
29  
30 Conversely, Taxol<sup>IV</sup> and Taxol<sup>SC</sup> led to significant ulceration and necrosis of the mice skin  
31 tissue at 60 mg.kg<sup>-1</sup> (see black arrows in Figure 4b), in agreement with the literature.<sup>49</sup>  
32  
33 Histopathological examination of HES-stained sections of skin samples removed at the  
34 injection site confirmed the above-mentioned macroscopic observations (Figure 4c). SC  
35 administration of the different polymer prodrugs evidenced a preserved architectural structure  
36 of the skin/SC tissue, with only focal small granulomatous lesion along needle tract. Neither  
37 significant degenerative or necrotic tegumentary changes were observed, nor inflammatory  
38 reaction, associated with the polymer prodrugs injection. On the contrary, Taxol<sup>IV</sup> and  
39 especially Taxol<sup>SC</sup> induced marked to severe ulcerative dermatitis with epidermal changes  
40 including hyperplasia and hyperkeratosis or severe epidermal-dermal necrosis replaced by a  
41 sero-cellular crust. Deep dermal and hypodermal inflammation was observed, granulomatous  
42 and/or granulocytic, associated with pannicular cytosteatonecrosis. Altogether, these results  
43  
44  
45  
46  
47  
48  
49  
50  
51  
52  
53  
54  
55  
56  
57  
58  
59  
60

1  
2  
3 establish for the first time the possibility to safely administer a vesicant/irritant anticancer drug  
4  
5 by SC injection.  
6  
7  
8  
9

### 10 **Pharmacokinetics and biodistribution**

11  
12 The biological fate of the prodrugs was then evaluated in terms of pharmacokinetics and  
13  
14 biodistribution in mice. A first pharmacokinetic study based on LC-MS/MS allowed to follow  
15  
16 the evolution in time of the Ptx concentration coming from Taxol<sup>IV</sup> or released from the  
17  
18 prodrugs at 7 mg.kg<sup>-1</sup> equiv. Ptx after SC administration. Taxol<sup>IV</sup> exhibited a high C<sub>max</sub> of 4 660  
19  
20 ng.mL<sup>-1</sup> 15 min post-administration (*t*<sub>max</sub>) followed by rapid clearance with undetectable  
21  
22 amounts in plasma after 24 h (Figure 5a), in good agreement with previous pharmacokinetic  
23  
24 studies of Taxol.<sup>50</sup> Conversely, the C<sub>max</sub> values of **P3d<sup>SC</sup>**, **P3e<sup>SC</sup>** and **P3c<sup>SC</sup>** were lowered by at  
25  
26 least an order of magnitude, to reach 310, 105 and 41 ng.mL<sup>-1</sup>, respectively (Table 2). These  
27  
28 results are in agreement with the MTD of the prodrugs from the toxicity study (Figure 4), as  
29  
30 lower C<sub>max</sub> values led to decreased toxicity and thus enabled a higher MTD than Taxol.<sup>48, 51-52</sup>  
31  
32 Interestingly, the C<sub>max</sub> values were observed at ~1-2 h (*t*<sub>max</sub>) for all prodrugs. This delayed *t*<sub>max</sub>  
33  
34 compared to that of Taxol<sup>IV</sup> is attributed to the time required for the prodrugs to be absorbed  
35  
36 into the blood or lymphatic capillaries, combined with the prolonged release of Ptx from the  
37  
38 prodrugs once they reach the bloodstream. Notably, **P3e<sup>SC</sup>** showed a very different PK profile  
39  
40 to the other prodrugs and Taxol<sup>IV</sup>. Whereas the elimination half-lives (*t*<sub>1/2</sub>) of **P3d<sup>SC</sup>**, **P3c<sup>SC</sup>** and  
41  
42 Taxol<sup>IV</sup> were in the range of 1.5–1.7 h, *t*<sub>1/2</sub> of **P3e<sup>SC</sup>** approached 14 h and it was detectable for  
43  
44 more than 3 days. The mean residence time (MRT) was also much higher for **P3e<sup>SC</sup>** (22.2 h vs.  
45  
46 0.9–3.3 h).  
47  
48  
49  
50  
51  
52  
53  
54  
55  
56  
57  
58  
59  
60

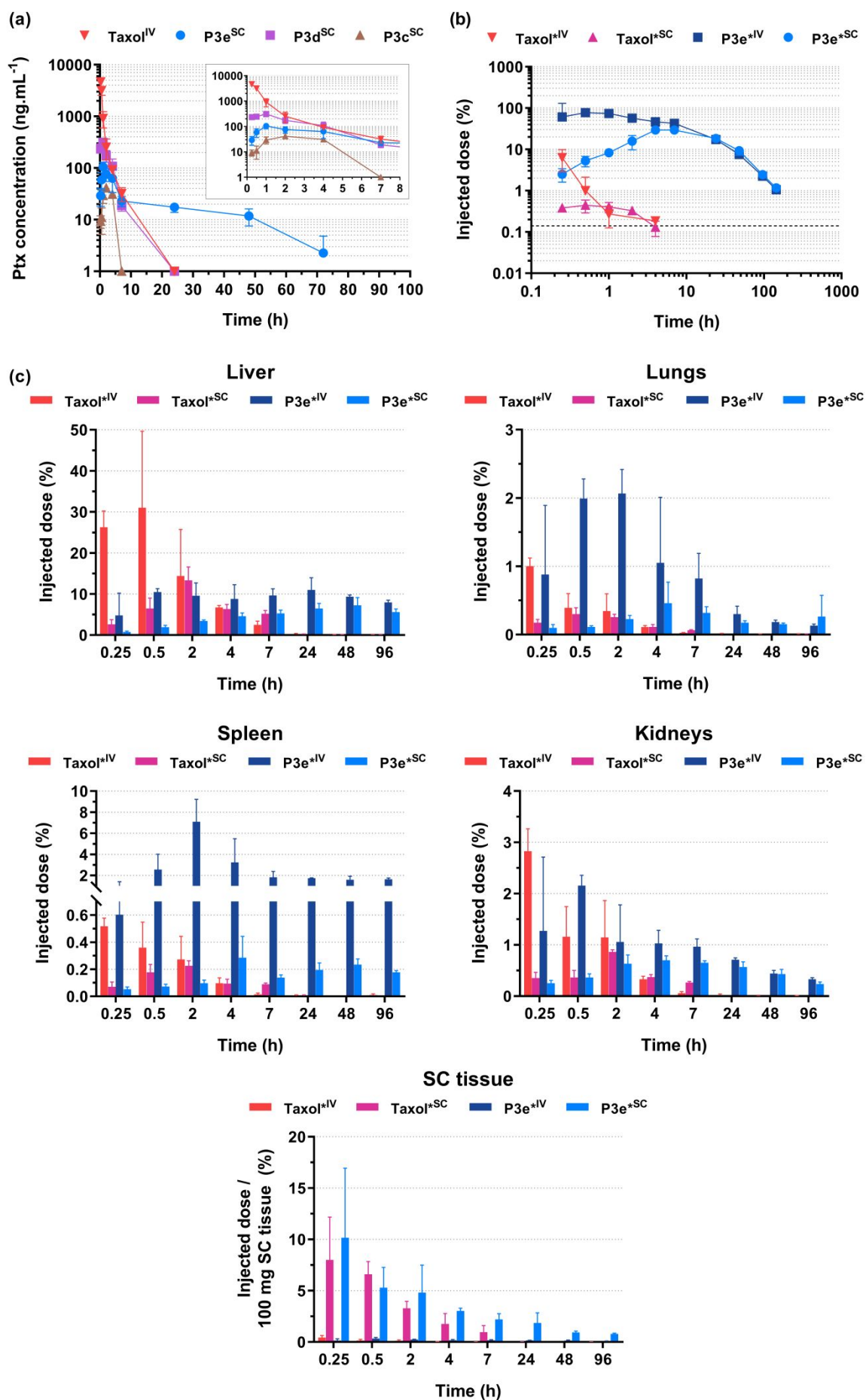


**Figure 5.** (a) Plasma concentration of free Ptx with time after injection of Taxol<sup>IV</sup>, Taxol<sup>SC</sup>, **P3e<sup>SC</sup>**, **P3d<sup>SC</sup>** and **P3c<sup>SC</sup>** at 7 mg.kg<sup>-1</sup> equiv. Ptx determined by LC-MS/MS (insert: zoomed-in region in the 0–10 h range). The values are expressed as the means ± SD (n = 4). (b) Plasma concentration and (c) biodistribution (in the liver, lungs, spleen, kidneys and SC tissue) with time of total Ptx after injection of Taxol<sup>IV</sup>, Taxol<sup>SC</sup>, **P3e<sup>IV</sup>** and **P3e<sup>SC</sup>** at 7 mg.kg<sup>-1</sup> equiv. Ptx determined by radioactive counting. The values are expressed as the means ± SD (n = 4). The horizontal dashed line represents the limit of quantification (0.14%)

**Table 2.** Main pharmacokinetic parameters of free Ptx determined by LC-MS/MS after IV injection of Taxol (Taxol<sup>IV</sup>) at 7 mg.kg<sup>-1</sup> and after SC injection of **P3d<sup>SC</sup>**, **P3e<sup>SC</sup>** and **P3c<sup>SC</sup>** at 7 mg.kg<sup>-1</sup> (Ptx equiv.).

Parameter	Taxol <sup>IV</sup>	<b>P3d<sup>SC</sup></b>	<b>P3e<sup>SC</sup></b>	<b>P3c<sup>SC</sup></b>
$t_{1/2}$ (h)	1.7	1.5	13.9	1.6
$t_{max}$ (h)	0.25	1	1	2
$C_{max}$ (ng.mL <sup>-1</sup> )	4 657	310	105	41
$AUC_{0 \rightarrow \infty}$ (ng.mL <sup>-1</sup> .h)	4 631	986	1 299	186
MRT (h)	0.9	2.5	22.2	3.3
Apparent bioavailability <sup>a</sup> (%)	100	21	28	4

<sup>a</sup> Determined according to  $AUC_{0 \rightarrow \infty} / AUC_{0 \rightarrow \infty} IV$ .

The apparent bioavailability of Ptx for **P3d<sup>SC</sup>**, **P3e<sup>SC</sup>** and **P3c<sup>SC</sup>** amounted to 21%, 28%, and 4% relative to Taxol IV, respectively (Table 2). This makes **P3e<sup>SC</sup>** the best candidate as it possessed both the most suitable PK profile and the highest apparent bioavailability. Despite similar apparent bioavailability for **P3e<sup>SC</sup>** and **P3d<sup>SC</sup>**, **P3d<sup>SC</sup>** exhibited a lower MRT and rapid release of Ptx once in the blood, leading to a too rapid clearance of the drug. For **P3e<sup>SC</sup>**, Ptx was released too slowly and the prodrug was therefore excreted before it could effectively release its payload. The optimal performance of **P3e<sup>SC</sup>** could be explained by its intermediate Ptx release profile in vivo (probably due to the presence of specific enzymes such as esterases), combined with the stealth properties provided by PAAm.<sup>22-23, 53</sup> This resulted in a long circulating prodrug acting as a slow-release reservoir of Ptx. These results are important not only because they confirm that the nature of the linker plays a key role in the pharmacokinetics

1  
2  
3 of Ptx, but also because they show that bioavailability does not correlate linearly with the drug  
4  
5 release pattern and thus screening each prodrug in vivo was necessary.  
6  
7

8 **P3e** was then selected for further study. A radiolabeled counterpart (**P3e\***) was  
9  
10 synthesized from [ $H^3$ ]-Ptx and used in a second pharmacokinetic study at the same dose to  
11  
12 monitor the whole amount of Ptx in comparison to that of radiolabeled Taxol\* (Figure 5b).  
13  
14 Since quantification is performed by radioactivity counting, free [ $H^3$ ]-Ptx, **P3e\*** and their  
15  
16 metabolites were dosed all together, which allows the fate of the prodrug to be followed. Free  
17  
18 [ $H^3$ ]-Ptx administered intravenously (Taxol\*<sup>IV</sup>) was rapidly cleared from the blood  
19  
20 compartment (<1% of the injected dose still circulating at 30 min post-injection, Figure 5b) and  
21  
22 exhibited most of the pharmacokinetic parameters similar to those previously observed by LC-  
23  
24 MS/MS (Table 2). In comparison, Taxol\*<sup>SC</sup> showed a delayed entrance into the blood  
25  
26 circulation, as shown by its very low  $C_{max}$  (< 1% of the injected dose) and bioavailability of  
27  
28 25%. Ptx from IV-injected **P3e\*** (**P3e\*<sup>IV</sup>**) has a prolonged circulation time with  $t_{1/2}$  10 times  
29  
30 and an AUC 100 times greater than Taxol\*<sup>IV</sup> (Table S2). Remarkably, Ptx from SC-injected  
31  
32 **P3e\*** (**P3e\*<sup>SC</sup>**) exhibited a high bioavailability (84% relative to **P3e\*<sup>IV</sup>**) and a total dose slowly  
33  
34 increasing over time, from 3% of the injected dose 15 min post-injection up to 46% after 4 h.  
35  
36 Once in the blood compartment, the prodrug remained in circulation for a prolonged period of  
37  
38 time (MRT ~36 h), with a final Ptx blood concentration of still ~1% of the injected dose 6 days  
39  
40 after injection, similarly to that of **P3e\*<sup>IV</sup>**. It is worth noting that **P3e\*<sup>SC</sup>** and **P3e\*<sup>IV</sup>** exhibited  
41  
42 the same  $t_{1/2}$  value of ~25 h, revealing that absorption rate is not significant after 24 h,  
43  
44 suggesting quantitative absorption of **P3e\*<sup>SC</sup>** into the blood within this period of time.  
45  
46  
47  
48  
49  
50

51 From the biodistribution study into key organs, both **P3e\*<sup>SC</sup>** and **P3e\*<sup>IV</sup>** showed very  
52  
53 limited accumulation in the liver (< 10% of the injected dose) 48 h post-injection, compared to  
54  
55 30% of the injected dose for Taxol\*<sup>IV</sup> after 30 min, presumably as a result of the stealth  
56  
57 properties of the prodrugs (Figure 5c). For other organs (lungs, spleen, kidneys), the total  
58  
59  
60

1  
2  
3 concentrations of Ptx from **P3e<sup>SC</sup>**, **P3e<sup>IV</sup>** and Taxol<sup>IV</sup> were low and in the same range (except  
4  
5 a modest accumulation of **P3e<sup>IV</sup>** in the spleen), revealing no noticeable acute toxicity. The  
6  
7 total amount of Ptx from **P3e<sup>SC</sup>** was also monitored in the SC tissue. It decreased sharply over  
8  
9 time, in parallel with an increase in the bloodstream, as shown from the pharmacokinetic profile  
10  
11 (Figure 5c). The SC data further prove the rapid blood passage of the hydrophilic prodrug from  
12  
13 the SC tissue. Overall, taking into account the PK/BD data and the toxicity study, these results  
14  
15 argue for efficacy studies of **P3e<sup>SC</sup>** in mouse tumor models.  
16  
17  
18  
19  
20

### 21 **Anticancer efficacy**

22  
23 An efficacy study was then designed to address two important points. Will **P3e<sup>SC</sup>** be as efficient  
24  
25 as Taxol<sup>IV</sup> at the same dose? And if yes, can **P3e<sup>SC</sup>** outperform Taxol<sup>IV</sup> at a higher dose thanks  
26  
27 to its higher MTD?  
28  
29

30  
31 In this context, mice bearing MCF-7 xenografts were treated with: (i) PAAm<sup>SC</sup> at 1520  
32  
33 mg.kg<sup>-1</sup>, which would correspond to 60 mg.kg<sup>-1</sup> equiv. Ptx for the prodrug counterpart; (ii)  
34  
35 Taxol<sup>IV</sup> at 15 mg.kg<sup>-1</sup>, determined to be the MTD for a weekly injection repeated over three  
36  
37 weeks and (iii) **P3e<sup>SC</sup>** at two different doses; either 15 mg.kg<sup>-1</sup> equiv. Ptx (to have the same  
38  
39 dose as for Taxol<sup>IV</sup>) or at a four-time higher dose of 60 mg.kg<sup>-1</sup> (determined to be the MTD in  
40  
41 equivalent Ptx of **P3e<sup>SC</sup>** for such a dose regimen). The antitumor efficacy of the different  
42  
43 treatments was evaluated by following the tumor growth (Figure 6a), from which two key  
44  
45 metrics used to characterize the antitumor activity were extracted:<sup>54</sup> the tumor volume over  
46  
47 control volume (T/C) (Figure 6b) and the tumor growth inhibition (TGI) (Figure 6c). The  
48  
49 overall survival of mice (Figure 6d) during the study and the mice body weight evolution  
50  
51 (Figure 6e) were also monitored.  
52  
53  
54  
55  
56  
57  
58  
59  
60



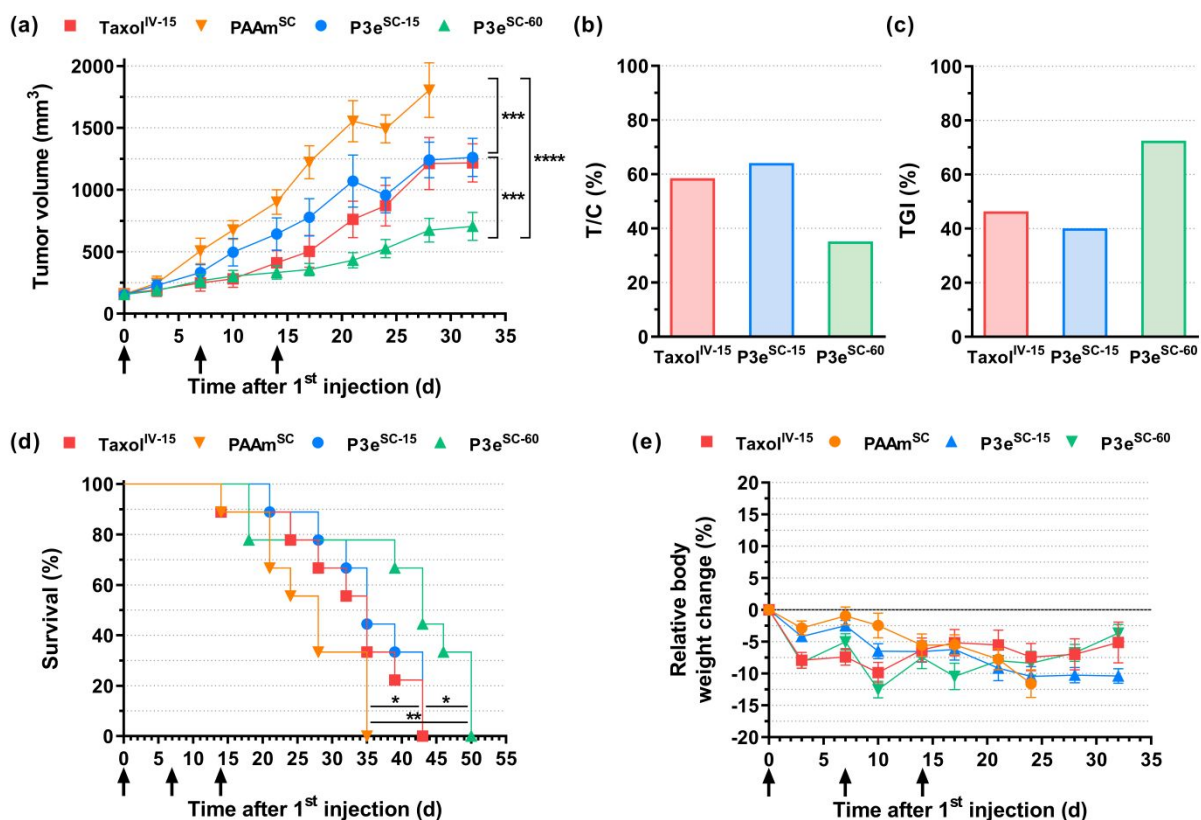


**Figure 6.** (a) Tumor growth evolution with time [the values are expressed as the means  $\pm$  SEM ( $n = 9$  per group)]. 2-Way ANOVA, with Tukey correction for multiple comparisons between groups at day 28 and 32; \*\*\* ( $p \leq 0.002$ ), \*\*\*\* ( $p < 0.0001$ ); (b) mean tumor volume over control volume (T/C) and (c) mean tumor growth inhibition (TGI) ten days after treatment termination ( $d = 24$  after 1<sup>st</sup> injection); (d) survival percentage evolution with time [Mantel-Cox test; \* ( $p < 0.05$ ), \*\* ( $p < 0.01$ )] and (e) weight evolution with time [the values are expressed as the means  $\pm$  SEM ( $n = 9$  per group)] of mice bearing MCF-7 xenografts after injection of Taxol<sup>IV</sup>, PAAm<sup>SC</sup> at 1520 mg.kg<sup>-1</sup>, P3e<sup>SC</sup> at 15 mg.kg<sup>-1</sup> (P3e<sup>SC-15</sup>) and P3e<sup>SC</sup> at 60 mg.kg<sup>-1</sup> (P3e<sup>SC-60</sup>) equiv. Ptx, on days 0, 7 and 14 (black arrows).

PAAm<sup>SC</sup>-treated mice exhibited rapid tumor growth with an average tumor volume exceeding 1500 cm<sup>3</sup> ~40 days post-tumor induction (Figure 6a and S7). Conversely, Taxol<sup>IV</sup> and P3e<sup>SC</sup> at 15 mg.kg<sup>-1</sup> both showed similar anticancer activity as attested by reduction on tumor growth compared to PAAm<sup>SC</sup> (Figure 6a and S7), together with similar T/C (59–64%) and TGI (40–46%) values ten days after treatment termination (Figures 6b and 6c, Tables S2 and S3). This first result is of crucial importance as, despite the lower apparent bioavailability of Ptx from P3e<sup>SC</sup> (Table 2), the efficacy study revealed that it had a similar antitumoral activity as Taxol<sup>IV</sup>

1  
2  
3 at the same dose. In combination with the toxicity data, this suggested a successful and safe  
4 transposition from IV-injected Taxol to SC-injected Ptx in the form of a water-soluble polymer  
5 prodrug.  
6  
7  
8  
9

10 Remarkably, when **P3e**<sup>SC</sup> was administered at a higher dose of 60 mg.kg<sup>-1</sup> equiv. Ptx, it  
11 displayed a dose-dependent anticancer activity and outperformed Taxol<sup>IV</sup> (Figure 6a and S7)  
12 with a T/C as low as 35% and a much higher TGI value of 73% ten days after treatment  
13 termination (Figures 6b and 6c, Tables S2 and S3). Consequently, not only was SC  
14 administration of **P3e** successful, but it could also induce greater anticancer activity than  
15 Taxol<sup>IV</sup> thanks to its higher MTD.  
16  
17  
18  
19  
20  
21  
22

23 In terms of overall survival of mice (Figure 6d), **P3e**<sup>SC</sup> administered at 60 mg.kg<sup>-1</sup> equiv.  
24 Ptx led to the highest survival rate of 78%, 25 days after treatment termination, whereas it was  
25 44% for **P3e**<sup>SC</sup> at 15 mg.kg<sup>-1</sup>, only 33% for Taxol<sup>IV</sup> and 0% for the control group (PAAm<sup>SC</sup>).  
26 As a result, **P3e**<sup>SC</sup> more than doubled the survival rate compared to Taxol<sup>IV</sup>. The evolution of  
27 the relative body-weight loss in **P3e**<sup>SC</sup>-treated mice also revealed that the treatment was well  
28 tolerated as mice lost no more than 10 % of their body weight throughout the efficacy study  
29 (Figure 6e).  
30  
31  
32  
33  
34  
35  
36  
37  
38  
39  
40  
41  
42

## 43 Conclusion

44  
45  
46 In this work, we presented a novel and general approach for the SC administration of  
47 irritant/vesicant anticancer drugs via the design of well-defined hydrophilic polymer prodrugs  
48 constructed by the “drug-initiated” method. To validate our strategy, we applied it to the  
49 anticancer drug Ptx as a worst-case scenario due to its high hydrophobicity and vesicant nature,  
50 while PAAm was chosen due to its high hydrophilicity and stealth properties. We first  
51 synthesized a small library of Ptx-based polymer prodrugs by screening different linkers (ester,  
52  
53  
54  
55  
56  
57  
58  
59  
60

1  
2  
3 diglycolate and carbonate) and choosing the appropriate chain length ( $M_n \sim 20 \text{ kg}\cdot\text{mol}^{-1}$ ) to  
4 obtain fully water-soluble polymer prodrugs. We then performed a comprehensive preclinical  
5 development of these polymer prodrugs by studying their physicochemical properties, drug  
6 release kinetics on two different cancer cell lines and acute local and systemic toxicity, as well  
7 as their pharmacokinetic and biodistribution profiles, and anticancer efficacy in tumor-bearing  
8 mice of the most promising candidate (i.e., Ptx-*ester*-PAAm). We demonstrated that SC  
9 injection of hydrophilic polymer prodrugs based on Ptx as a representative vesicant/irritant  
10 anticancer drug allowed sustained release of Ptx in the bloodstream and outperformed the  
11 anticancer efficacy of Taxol, the commercial formulation of Ptx, without inducing local  
12 toxicity.  
13  
14  
15  
16  
17  
18  
19  
20  
21  
22  
23  
24  
25

26           Given the flexibility of the synthetic approach, these achievements pave the way for SC  
27 administration of a wide range of anticancer drugs, including irritant and vesicant ones, and  
28 make it possible to safely consider the translation of many IV chemotherapies to SC  
29 chemotherapies. From a more general perspective, this new drug-delivery platform could also  
30 represent an important step towards self-administration and chemotherapy at home, which  
31 would greatly increase patient comfort and reduce the high cost of cancer treatment; the latter  
32 being crucial for low- and middle-income countries.  
33  
34  
35  
36  
37  
38  
39  
40  
41  
42  
43  
44

## 45 **Acknowledgments**

46  
47  
48 This project has received funding from the European Research Council (ERC) under the  
49 European Union's Horizon 2020 research and innovation programme (Grant agreement No.  
50 771829). We thank la Ligue contre le Cancer for the financial support of the PhD thesis of AB,  
51 Université Paris-Saclay Prématuration for the funding of TB and CNRS Prématuration and  
52 SATT Paris-Saclay for the funding of NI. We also thank Camille Dejean (BioCIS, Université  
53 Paris-Sud), Assia Hessani (IGPS, Université Paris-Saclay) for technical assistance in NMR  
54 spectroscopy and radioactivity experiments, respectively. The CNRS is also acknowledged for  
55 financial support.  
56  
57  
58  
59  
60

## References

1. Stewart, B. W.; Wild, C. P., *World Cancer Report 2014*. International Agency for Research on Cancer: 2014.
2. Weir, H. K.; Thompson, T. D.; Soman, A.; Møller, B.; Leadbetter, S.; White, M. C., Meeting the Healthy People 2020 Objectives to Reduce Cancer Mortality. *Prev. Chronic Dis.* **2015**, *12*.
3. Mariotto, A. B.; Robin Yabroff, K.; Shao, Y.; Feuer, E. J.; Brown, M. L., Projections of the Cost of Cancer Care in the United States: 2010–2020. *J. Natl. Cancer Inst.* **2011**, *103* (2), 117-128.
4. <https://www.drugwatch.com/2015/10/07/cost-of-cancer>
5. Aitken, M., *Global Oncology Trend Report*. IMS Institute for Healthcare Informatics: 2016.
6. Koh, D. B. C.; Gowardman, J. R.; Rickard, C. M.; Robertson, I. K.; Brown, A., Prospective study of peripheral arterial catheter infection and comparison with concurrently sited central venous catheters. *Crit. Care Med.* **2008**, *36* (2), 397-402.
7. Pujol, M.; Hornero, A.; Saballs, M.; Argerich, M. J.; Verdaguer, R.; Císnal, M.; Peña, C.; Ariza, J.; Gudiol, F., Clinical epidemiology and outcomes of peripheral venous catheter-related bloodstream infections at a university-affiliated hospital. *J. Hosp. Infect.* **2007**, *67* (1), 22-29.
8. Jin, J. F.; Zhu, L. L.; Chen, M.; Xu, H. M.; Wang, H. F.; Feng, X. Q.; Zhu, X. P.; Zhou, Q., The optimal choice of medication administration route regarding intravenous, intramuscular, and subcutaneous injection. *Patient Prefer. Adherence* **2015**, *9*, 923-42.
9. Pivot, X.; Gligorov, J.; Müller, V.; Barrett-Lee, P.; Verma, S.; Knoop, A.; Curigliano, G.; Semiglazov, V.; López-Vivanco, G.; Jenkins, V.; Scotto, N.; Osborne, S.; Fallowfield, L., Preference for subcutaneous or intravenous administration of trastuzumab in patients with HER2-positive early breast cancer (PrefHer): an open-label randomised study. *Lancet Oncol.* **2013**, *14* (10), 962-970.
10. Leveque, D., Subcutaneous Administration of Anticancer Agents. *Anticancer Res.* **2014**, *34* (4), 1579-1586.
11. Sequeira, J. A. D.; Santos, A. C.; Serra, J.; Estevens, C.; Seíça, R.; Veiga, F.; Ribeiro, A. J., Subcutaneous delivery of biotherapeutics: challenges at the injection site. *Expert Opin. Drug Deliv.* **2019**, *16* (2), 143-151.
12. Laza-Knoerr, A. L.; Gref, R.; Couvreur, P., Cyclodextrins for drug delivery. *J. Drug Targeting* **2010**, *18* (9), 645-656.
13. Heise, T.; Meiffren, G.; Alluis, B.; Seroussi, C.; Ranson, A.; Arrubla, J.; Correia, J.; Gaudier, M.; Soula, O.; Soula, R.; DeVries, J. H.; Klein, O.; Bode, B., BioChaperone Lispro versus faster aspart and insulin aspart in patients with type 1 diabetes using continuous subcutaneous insulin infusion: A randomized euglycemic clamp study. *Diabetes Obes. Metab.* **2019**, *21* (4), 1066-1070.
14. Frost, G. I., Recombinant human hyaluronidase (rHuPH20): an enabling platform for subcutaneous drug and fluid administration. *Expert Opin. Drug Deliv.* **2007**, *4* (4), 427-440.
15. McLennan, D. N.; Porter, C. J. H.; Charman, S. A., Subcutaneous drug delivery and the role of the lymphatics. *Drug Discov. Today Technol.* **2005**, *2* (1), 89-96.
16. Chen, W.; Yung, B. C.; Qian, Z.; Chen, X., Improving long-term subcutaneous drug delivery by regulating material-bioenvironment interaction. *Adv. Drug Delivery Rev.* **2018**, *127*, 20-34.
17. Oussoren, C.; Storm, G., Liposomes to target the lymphatics by subcutaneous administration. *Adv. Drug Delivery Rev.* **2001**, *50* (1–2), 143-156.
18. Barbee, M. S.; Owonikoko, T. K.; Harvey, R. D., Taxanes: vesicants, irritants, or just irritating? *Ther. Adv. Med. Oncol.* **2013**, *6* (1), 16-20.

19. Shenaq, S. M.; Abbase, E.-H. A.; Friedman, J. D., Soft-tissue Reconstruction Following Extravasation of Chemotherapeutic Agents. *Surg. Oncol. Clin. N. Am.* **1996**, *5* (4), 825-846.
20. Alley, E.; Green, R.; Schuchter, L., Cutaneous toxicities of cancer therapy. *Curr. Opin. Oncol.* **2002**, *14* (2).
21. Boyle, D. M.; Engelking, C., Vesicant extravasation: myths and realities. *Oncol. Nurs. Forum* **1995**, *22* (1), 57-67.
22. Kaneda, Y.; Tsutsumi, Y.; Yoshioka, Y.; Kamada, H.; Yamamoto, Y.; Kodaira, H.; Tsunoda, S.-i.; Okamoto, T.; Mukai, Y.; Shibata, H.; Nakagawa, S.; Mayumi, T., The use of PVP as a polymeric carrier to improve the plasma half-life of drugs. *Biomaterials* **2004**, *25* (16), 3259-3266.
23. Torchilin, V. P.; Shtilman, M. I.; Trubetsky, V. S.; Whiteman, K.; Milstein, A. M., Amphiphilic vinyl polymers effectively prolong liposome circulation time in vivo. *Biochim. Biophys. Acta - Biomembr.* **1994**, *1195* (1), 181-184.
24. Yamauchi, P. S., Emerging permanent filler technologies: focus on Aquamid. *Clin. Cosmet. Investig. Dermatol.* **2014**, *7*, 261-266.
25. Kinnunen, H. M.; Mrsny, R. J., Improving the outcomes of biopharmaceutical delivery via the subcutaneous route by understanding the chemical, physical and physiological properties of the subcutaneous injection site. *J. Control. Rel.* **2014**, *182*, 22-32.
26. Kingston, D. G. I., Taxol: The chemistry and structure-activity relationships of a novel anticancer agent. *Trends Biotechnol.* **1994**, *12* (6), 222-227.
27. Hertz, D. L.; Kidwell, K. M.; Vangipuram, K.; Li, F.; Pai, M. P.; Burness, M.; Griggs, J. J.; Schott, A. F.; Van Poznak, C.; Hayes, D. F.; Lavoie Smith, E. M.; Henry, N. L., Paclitaxel Plasma Concentration after the First Infusion Predicts Treatment-Limiting Peripheral Neuropathy. *Clin. Cancer Res.* **2018**, *24* (15), 3602-3610.
28. Bao, Y.; Guegain, E.; Mougin, J.; Nicolas, J., Self-stabilized, hydrophobic or PEGylated paclitaxel polymer prodrug nanoparticles for cancer therapy. *Polym. Chem.* **2018**, *9* (6), 687-698.
29. Burckbuchler, V.; Mekhloufi, G.; Giteau, A. P.; Grossiord, J. L.; Huille, S.; Agnely, F., Rheological and syringeability properties of highly concentrated human polyclonal immunoglobulin solutions. *Eur. J. Pharm. Biopharm.* **2010**, *76* (3), 351-356.
30. Zhang, Y.; Huo, M.; Zhou, J.; Xie, S., PKSolver: An add-in program for pharmacokinetic and pharmacodynamic data analysis in Microsoft Excel. *Comput. Methods Programs Biomed.* **2010**, *99* (3), 306-314.
31. Sonnichsen, D. S.; Liu, Q.; Schuetz, E. G.; Schuetz, J. D.; Pappo, A.; Relling, M. V., Variability in human cytochrome P450 paclitaxel metabolism. *J. Pharmacol. Exp. Ther.* **1995**, *275* (2), 566-75.
32. Gianni, L.; Kearns, C. M.; Giani, A.; Capri, G.; Viganó, L.; Lacatelli, A.; Bonadonna, G.; Egorin, M. J., Nonlinear pharmacokinetics and metabolism of paclitaxel and its pharmacokinetic/pharmacodynamic relationships in humans. *J. Clin. Oncol.* **1995**, *13* (1), 180-90.
33. Nicolas, J., Drug-Initiated Synthesis of Polymer Prodrugs: Combining Simplicity and Efficacy in Drug Delivery. *Chem. Mater.* **2016**, *28* (6), 1591-1606.
34. Harrison, S.; Nicolas, J.; Maksimenko, A.; Bui, D. T.; Mougin, J.; Couvreur, P., Nanoparticles with In Vivo Anticancer Activity from Polymer Prodrug Amphiphiles Prepared by Living Radical Polymerization. *Angew. Chem., Int. Ed.* **2013**, *52*, 1678-1682.
35. Bao, Y.; Boissenot, T.; Guégain, E.; Desmaële, D.; Mura, S.; Couvreur, P.; Nicolas, J., Simple Synthesis of Cladribine-Based Anticancer Polymer Prodrug Nanoparticles with Tunable Drug Delivery Properties. *Chem. Mater.* **2016**, *28* (17), 6266-6275.
36. Guégain, E.; Tran, J.; Deguettes, Q.; Nicolas, J., Degradable polymer prodrugs with adjustable activity from drug-initiated radical ring-opening copolymerization. *Chem. Sci.* **2018**, *9* (43), 8291-8306.

- 1  
2  
3 37. Louage, B.; Nuhn, L.; Risseeuw, M. D. P.; Vanparijs, N.; De Coen, R.; Karalic, I.; Van Calenbergh,  
4 S.; De Geest, B. G., Well-Defined Polymer–Paclitaxel Prodrugs by a Grafting-from-Drug  
5 Approach. *Angew. Chem., Int. Ed.* **2016**, *55* (39), 11791-11796.  
6  
7 38. Di Consiglio, E.; Darney, K.; Buratti, F. M.; Turco, L.; Vichi, S.; Testai, E.; Lautz, L. S.; Dorne, J.  
8 L. C. M., Human Variability in Carboxylesterases and carboxylesterase-related Uncertainty Factors  
9 for Chemical Risk Assessment. *Toxicol. Lett.* **2021**, *350*, 162-170.  
10  
11 39. Li, D., The Impact of Carboxylesterases in Drug Metabolism and Pharmacokinetics. *Curr. Drug*  
12 *Metab.* **2019**, *20* (2), 91-102.  
13  
14 40. Bao, Y.; De Keersmaecker, H.; Corneillie, S.; Yu, F.; Mizuno, H.; Zhang, G.; Hofkens, J.; Mendrek,  
15 B.; Kowalczyk, A.; Smet, M., Tunable Ratiometric Fluorescence Sensing of Intracellular pH by  
16 Aggregation-Induced Emission-Active Hyperbranched Polymer Nanoparticles. *Chem. Mater.*  
17 **2015**, *27* (9), 3450-3455.  
18  
19 41. D'Souza, A. J. M.; Topp, E. M., Release from polymeric prodrugs: Linkages and their degradation.  
20 *J. Pharm. Sci.* **2004**, *93* (8), 1962-1979.  
21  
22 42. Ragelle, H.; Danhier, F.; Pr eat, V.; Langer, R.; Anderson, D. G., Nanoparticle-based drug delivery  
23 systems: a commercial and regulatory outlook as the field matures. *Expert Opin. Drug Deliv.* **2017**,  
24 *14* (7), 851-864.  
25  
26 43. Joint FAO/WHO Consultation on Health Implications of Acrylamide in Food (2002 : Geneva,  
27 Switzerland) & WHO Food Safety Programme. (2002). Health implications of acrylamide in food  
28 : report of a joint FAO/WHO consultation, WHO Headquarters, Geneva, Switzerland, 25-27 June  
29 2002. World Health Organization  
30  
31 44. Panel, C. I. R. E., Amended Final Report on the Safety Assessment of Polyacrylamide and  
32 Acrylamide Residues in Cosmetics. *Int. J. Toxicol.* **2005**, *24* (2\_suppl), 21-50.  
33  
34 45. Watt, R. P.; Khatri, H.; Dibble, A. R. G., Injectability as a function of viscosity and dosing materials  
35 for subcutaneous administration. *Int. J. Pharm.* **2019**, *554*, 376-386.  
36  
37 46. Royer, I.; Alvinerie, P.; Wright, M.; Monsarrat, B.; Ho, L. K.; Armand, J. P., Paclitaxel metabolites  
38 in human plasma and urine: Identification of 6 $\alpha$ -hydroxytaxol, 7-epitaxol and taxol hydrolysis  
39 products using liquid chromatography/atmospheric-pressure chemical ionization mass  
40 spectrometry. *Rapid Commun. Mass Spectrom.* **1995**, *9* (6), 495-502.  
41  
42 47. Volk, K. J.; Hill, S. E.; Kerns, E.; Lee, M. S., Profiling degradants of paclitaxel using liquid  
43 chromatography–mass spectrometry and liquid chromatography–tandem mass spectrometry  
44 substructural techniques. *J. Chromatogr. B* **1997**, *696* (1), 99-115.  
45  
46 48. Rowinsky, E. K.; Donehower, R. C., The clinical pharmacology of paclitaxel (Taxol). *Semin.*  
47 *Oncol.* **1993**, *20* (4 Suppl 3), 16-25.  
48  
49 49. Dorr, R. T.; Snead, K.; Liddil, J. D., Skin ulceration potential of paclitaxel in a mouse skin model  
50 in vivo. *Cancer* **1996**, *78* (1), 152-156.  
51  
52 50. Shin, B. S.; Kim, H. J.; Hong, S. H.; Lee, J. B.; Hwang, S. W.; Lee, M. H.; Yoo, S. D., Enhanced  
53 absorption and tissue distribution of paclitaxel following oral administration of DHP 107, a novel  
54 mucoadhesive lipid dosage form. *Cancer Chemother. Pharmacol.* **2009**, *64* (1), 87-94.  
55  
56 51. Marupudi, N. I.; Han, J. E.; Li, K. W.; Renard, V. M.; Tyler, B. M.; Brem, H., Paclitaxel: a review  
57 of adverse toxicities and novel delivery strategies. *Expert Opin. Drug Saf.* **2007**, *6* (5), 609-21.  
58  
59 52. Nieto, Y.; Cagnoni, P. J.; Bearman, S. I.; Shpall, E. J.; Matthes, S.; DeBoom, T.; Bar on, A.; Jones,  
60 R. B., Acute encephalopathy: a new toxicity associated with high-dose paclitaxel. *Clin. Cancer*  
*Res.* **1999**, *5* (3), 501-6.  
61  
62 53. Knop, K.; Hoogenboom, R.; Fischer, D.; Schubert, U. S., Poly(ethylene glycol) in Drug Delivery:  
63 Pros and Cons as Well as Potential Alternatives. *Angew. Chem., Int. Ed.* **2010**, *49* (36), 6288-6308.

- 1  
2  
3 54. Zhu, A. Z., Quantitative translational modeling to facilitate preclinical to clinical efficacy &  
4 toxicity translation in oncology. *Future Science OA* **2018**, *4* (5), FSO306.  
5  
6  
7  
8  
9  
10  
11  
12  
13  
14  
15  
16  
17  
18  
19  
20  
21  
22  
23  
24  
25  
26  
27  
28  
29  
30  
31  
32  
33  
34  
35  
36  
37  
38  
39  
40  
41  
42  
43  
44  
45  
46  
47  
48  
49  
50  
51  
52  
53  
54  
55  
56  
57  
58  
59  
60